

Visibility in airborne volcanic ash: considerations for surface transportation using a laboratory-based method

Daniel M. Blake¹ · Thomas M. Wilson¹ · Carol Stewart²

Received: 22 June 2016 / Accepted: 1 February 2018
© The Author(s) 2018. This article is an open access publication

Abstract All modes of surface transportation can be disrupted by visibility degradation caused by airborne volcanic ash. Despite much qualitative evidence of low visibility on roads following historical eruptions worldwide, there have been few detailed studies that have attempted to quantify relationships between visibility conditions and observed impacts on network functionality and safety. In the absence of detailed field observations, such gaps in knowledge can be filled by developing empirical datasets through laboratory investigations. Here, we use historical eruption data to estimate a plausible range of ash-settling rates and ash particle characteristics for Auckland city, New Zealand. We propose and implement a new experimental set-up in controlled laboratory conditions, which incorporates a dual-pass transmissometer and solid aerosol generator, to reproduce these ash-settling rates and calculate visual ranges through the associated airborne volcanic ash. Our findings demonstrate that visibility is most impaired for high ash-settling rates (i.e. $> 500 \text{ g m}^{-2} \text{ h}^{-1}$) and particle size is deemed the most influential ash characteristic for visual range. For the samples tested (all $< 320 \text{ }\mu\text{m}$ particle diameter), visibility was restricted to $\sim 1\text{--}2 \text{ m}$ when ash settling was replicated for very high rates (i.e. $\sim 4000 \text{ g m}^{-2} \text{ h}^{-1}$) and was especially low when ash particles were fine-grained, more irregular in shape and lighter in colour. Finally, we consider potential implications for disruption to surface transportation in Auckland through comparisons with existing research which investigates the consequences of visual range reduction for other atmospheric hazards such as fog. This includes discussing how our approach might be utilised in emergency and transport management planning. Finally, we summarise strategies available

Electronic supplementary material The online version of this article (<https://doi.org/10.1007/s11069-018-3205-3>) contains supplementary material, which is available to authorized users.

✉ Daniel M. Blake
daniel.blake@canterbury.ac.nz

¹ Department of Geological Sciences, University of Canterbury, Private Bag 4800, Christchurch 8140, New Zealand

² Joint Centre for Disaster Research, Massey University/GNS Science, PO Box 756, Massey University Wellington Campus, Wellington 6140, New Zealand

for the mitigation of visibility degradation in environments contaminated with volcanic ash.

Keywords Vehicle · Road · Visual range · Experimental · Opacity · Transmissometer

1 Introduction

Reduced visibility may occur during primary volcanic ashfall or through the remobilisation and resuspension of existing fall deposits (Sparks et al. 1997; Baxter and Horwell 1999; USGS 2013; Folch et al. 2014) into the atmosphere by wind, vehicle movement, cleaning processes or other human activities. Both primary and remobilised ash may produce potential issues for transportation (Barsotti et al. 2010; Folch 2012; Wilson et al. 2014; Blake et al. 2016a, b, 2017a, b). There have been many cases where reduced visibility following volcanic eruptions has impacted surface transportation¹ function, particularly road (Table 1), but also rail, maritime and at airports, sometimes to near-total darkness (Blong 1982; Guffanti et al. 2009). For example, following the Mount St Helens eruption in 1980, “zero visibility” caused traffic to come to a standstill in several places including on Interstate 90 near Ellensburg in Washington, with visibility so poor that the authorities used flares to guide motorists to nearby schools and churches (Warrick 1981, p.19). Once the initial ashfall was over, it became imperative to control traffic movement through speed restrictions, spacing vehicles on roads and road closures to avoid vehicles creating “great clouds of ash” and again reducing visibility on the roads (Warrick 1981, p.20). Hundreds of accidents in the affected areas were attributed to the billowing of ash behind vehicles and associated loss in visibility (Blong 1984). More recently, following the eruption of Cordón Caulle, Chile, in 2011, visibility in neighbouring Argentina, where ash fell, was so low that several main roads including Route 40 (linking Bariloche city and the Neuquén province) were subsequently closed. This affected the transportation of people and freight at a national level (Folch et al. 2014). Vehicle headlights and brake lights are often reported to be ineffective in such conditions and barely visible to other drivers (Cole and Blumenthal 2004; Wilson et al. 2012a; USGS 2013). Disruption to rail and maritime transportation caused by poor visibility during ashfall and resulting in safety and navigational issues has also been documented (Johnston 1997; Wilson et al. 2012a). For example, rail operations were shutdown during the initial Mount St Helens 1980 ashfall due to reduced visibility (as well as health concerns), with substantial speed restrictions and inspections necessary in the following days (Warrick 1981; Blong 1984).

Despite the many impacts to surface transportation that have been documented (Table 1), there has been little quantitative analysis into the effects of airborne volcanic ash on reducing visibility and the subsequent consequences for network functionality and safety. Contemporary critical infrastructure management increasingly aims to optimise network performance during natural hazards, especially for non-damaging events, such as minor ashfalls (Wilson et al. 2014). Ash thickness has usually been the key measure of hazard intensity adopted in the past (Table 1), but is likely to be of little relevance when assessing visibility impacts. Airborne ash concentration and ash-settling rates are more important for such impacts. The lack of an evidence base implies that surface transportation operators typically can only make crude management decisions of either taking a

¹ The term *surface transportation* is used in this paper to refer to common modes of transportation on land and at sea (i.e. road, rail, airport and maritime). It excludes airborne aircraft.

Table 1 Historical records of visibility impacts on road following volcanic eruptions. Other occurrences described as general impacts to transportation, where impacts on visibility may have occurred but are not specified in the literature, are not shown

Volcano (Year)	Ash thickness (mm)	Initial ashtfall visibility observations	Resuspended ash visibility observations	Mitigation measures	References
Ruapehu (1945)	"Few mm"	Reduced visibility on roads was common Ash made streetlights hazy	Bus headlamps blacked out by thick ash Recently deposited ash easily lifted by passing vehicles Resuspended ash similar to dust produced on unsealed roads	Road closures Drivers reduced speeds (to as low as $\sim 25 \text{ km h}^{-1}$) Ash removal Rain improved visibility	Johnston (1997)
St Helens (1980)	< 50	Traffic reduced to a virtual standstill because of zero visibility Gravel and sealed roads had similar visibility problems Flares had to be used to guide people	Ash billowing up behind fast-moving vehicles reduced visibility and likely caused hundreds of accidents Bus services shutdown and then limited services	Road closures Stricter speed limits Convoys Restrictions on vehicle type and numbers Advice not to drive except in emergencies Speed bumps constructed from ash Ash removal with some dampening first	Sarkinen and Wiitala (1981), Warrick (1981), Blong (1984); Johnston (1997)
Hudson (1991)	20–50		$\sim 1 \text{ m}$ visual range a week after eruption ("transport virtually closed down") Poor visibility on main coastal highway for up to a month	Road closures Rainfall contributed to ash hazards diminishing People avoided going outside Cleaning of streets prioritised	Wilson et al. (2009), Wilson (2009) (unpublished field notes)
	200–300	People could not drive partly due to visibility Ashtfall blocked sun and visibility was as low as 1 m in daytime			

Table 1 continued

Volcano (Year)	Ash thickness (mm)	Initial ashfall visibility observations	Resuspended ash visibility observations	Mitigation measures	References
Spurr (1992)	3	Ash limited visibility on roads	Bus services shutdown and then limited service	City trimmed bus schedules and sent 40% of workforce home Rain alleviated issues	Johnston (1997), Barnard (2009)
Unzen (1992)		Visibility reduced on roads by suspended ash			Yanagi et al. (1992), Barnard (2009)
Ruapehu (1995–1996)	“Thin”	Reduced visibility	Visibility on roads commonly reduced after ashfalls	Nearby state highway closed three times Diversions Ash removal	Johnston (1997), Barnard (2009)
Etna (2002)	< 2		Ash remobilisation by traffic and wind caused reduced visibility		Barnard (2009)
Chaitén (2008)		Reduced visibility “to nil” meant that maintenance crews were unable to traverse the access road to a hydroelectric dam	Visibility issues from vehicles travelling too fast (~ 50 m visual range in places)	Roads restricted by army to emergency vehicle use only Some roads made one-way to reduce accidents Permanent crew at dam for 1 month (rather than shifts) to reduce remobilisation Drivers reduced speeds Headlights used Rain alleviated issues	Wilson et al. (2012b), Wilson (2008) (unpublished field notes)
Pacaya (2011)	~ 300 20–30	10–15 m visibility Difficult to drive due to impaired visibility		Ash removal Rain helped consolidate tephra	Wardman et al. (2012)

Table 1 continued

Volcano (Year)	Ash thickness (mm)	Initial ashfall visibility observations	Resuspended ash visibility observations	Mitigation measures	References
Cordón Caulle (2011)			Low visibility led to difficult driving conditions for 2 weeks and accidents Visibility reduction meant no urban clean-up for a week in places	Road closures Lower speed enforcement and recommendations (some 20 km h ⁻¹) Ash dampened with water Ash removal	Wilson et al. (2013), Folch et al. (2014), Craig et al. (2016)
Shinmoedake (2011)	> 100	“No visibility”—decreased visibility Reduced visibility	Visibility problems lasted for some time	Roads closed Rapid clean-up operation Headlights used	Magrill et al. (2013) GVP (2013)
San Cristóbal (2013)		Visibility greatly reduced ~ 15 km from vent			
Kelud (2014)		Reduced visibility	Accident rates increased up to 220 km from vent Bus services shutdown and then limited service	Advice to not drive if possible Headlights used Drivers reduced speeds Ash removal Rain improved visibility	Blake et al. (2015)
Calbuco (2015)	~ 50	Visibility reduced to 500 m ~ 100 km from vent	500 m visual range recorded ~ 500 km from vent 3 days after last eruptive pulse		AccuWeather (2015), Reckziegel et al. (2016)

precautionary approach of shutting systems down in the presence of ash (or in the event of forecasted ash), or a reactive approach if airborne ash causes problems for a surface transportation system. However, several contemporary ash dispersion and fallout forecasting models, which are outlined in detail by Scollo et al. (2008) and Folch (2012), can provide outputs that include atmospheric concentrations and settling rates (e.g. FLEXPART—Stohl et al. 1998, 2005; VOL-CALPUFF—Barsotti et al. 2008; FALL3D—Costa et al. 2006; Folch et al. 2009). Therefore, the capacity now exists for surface transportation vulnerability assessments to adopt these metrics. Furthermore, settling rate and airborne concentration are important metrics to consider for other impacts to transportation. For example, it has been determined that concentrations as low as $1 \times 10^{-4} \text{ g m}^{-3}$ can cause substantial damage to aircraft (Witham et al. 2007; Folch and Sulpizio 2010).

In this paper, we next present a background section which summarises the interdisciplinary literature including the physical properties of volcanic ash, visibility degradation and surface transportation impacts. The background section also includes a summary of our Auckland case study site, which gives context to the work through the application of experimental processes and replication of ash types/colours, particle sizes and settling rates expected in the city from various volcanic sources. We then outline the methods used to simulate volcanic ashfall in a laboratory setting to investigate the effect of ash characteristics and settling rate on visibility degradation. Precise and consistent ash-generation rates (g h^{-1}) are produced in a purpose-built container using a Solid Aerosol Generator (*Topas SAG 410*). We also use a dual-pass transmissometer (*Dynoptic DSL-460 MkII*) for the measurement of opacity as a proxy for particulate emissions. We use datasets containing ash characteristic and geospatial information from the literature available following worldwide historical eruptions to test our methodology, specifically focusing on the Auckland case study. Results from the experimental tests are presented before a discussion of the findings related to visibility in airborne ash and forecasts for Auckland. Finally, we discuss key limitations of the experimental approach, provide suggestions for future work and suggest evidence-based, semi-quantitative transportation mitigation strategies that could be implemented in operational environments.

2 Background

2.1 Ash deposit thickness and visibility relationship

Ash deposit thickness is the most frequently (and often only) reported hazard intensity metric following volcanic eruptions (Pyle 1989; Wilson et al. 2012a, 2014, 2017; Blake et al. 2017a, b). There is generally a decreasing trend in ash thickness with distance from eruptive vents, although other spatial variations are possible due to ash aggregation and/or an unusually large proportion of mid-sized particles, which can lead to secondary maxima on a thickness versus distance plot (see Carey and Sigurdsson 1982; Pyle 1989; Sparks et al. 1992; Scasso et al. 1994; Bonadonna et al. 1998; Bonadonna and Phillips 2003; Bonadonna and Houghton 2005; Costa et al. 2009; Parfitt and Wilson 2009; Bonasia et al. 2012; Folch et al. 2010; Macedonio et al. 2016). Ash deposit thickness is clearly an important parameter for certain transportation impact types at quite low levels. For example, line marking coverage and loss of skid resistance on roads can occur with 0.1–1.0-mm-thick ash in some situations (Blake et al. 2016a, b, 2017a, b). However, ash thickness is generally a poor indicator for estimating likely effects on visibility. Some

studies indicate that thickness plays a minimal role in controlling airborne ash concentration, initial levels of visibility degradation and associated impact to transportation (e.g. Warrick 1981; Blong 1982). For example, reporting on the Mount St Helens 1980 eruption, Warrick (1981) states that “ash depth had little influence on the initial level of impact on the transportation systems”. Conversely, other studies suggest that thickness can be used to inform visibility impacts to a degree (e.g. Thorarinsson 1971; Johnston 1997; Searl et al. 2002). While there is potential for uncompacted fine ash to become airborne by disturbance of the deposit, and thicker deposits can prolong the duration of such remobilisation and subsequent recovery time (Searl et al. 2002; Hincks et al. 2006; Wilson et al. 2011), we propose that *ash-settling rate*² (especially for direct ashfall) and airborne particle concentration³ (for both direct and resuspended ash) are more appropriate metrics to adopt when assessing visibility impairment in environments containing volcanic ash. Therefore, the thicknesses outlined in Table 1 have little direct link to the visibility observations and should only be used as a loose proxy for airborne ash concentration and duration of exposure.

2.2 Volcanic ash-settling rate

Two fundamental processes affect ash-settling rate, which are depicted in Fig. 1:

- 1) Primary ashfall from the eruptive vent, which is the result of explosive volcanic eruptions causing the disintegration of magma or vent material and production of rock fragments (Jenkins et al. 2014). The *terminal fall velocity*⁴ of sedimenting particles affects ash-settling rate and is mainly dependent on their diameter, densities and, to some extent, their shape (see: Bonadonna et al. 1998; Riley et al. 2003; Parfitt and Wilson 2009; Pardini et al. 2016).
- 2) The remobilisation and resuspension of existing ash into the atmosphere from entrainment by meteorological winds, small-scale atmospheric turbulence caused by vehicle movement, cleaning processes and/or other human activities. The quantity of volcanic ash which becomes resuspended is dependent on the particle size, density, water content, shape, roughness of the ground material on which it has settled, and the degree of binding and compaction (Fowler and Lopushinsky 1986; Sivakumar 2005; Wilson et al. 2011)

We suggest that different ash-settling rates can be established under laboratory conditions. However, compared to other hazard intensity metrics such as ash thickness and

² Settling rate is defined here as the mass of particles falling onto a surface over time ($\text{g m}^{-2} \text{h}^{-1}$). However, we note that settling rate may also be referred to as *ash-deposition rate* or *ash accumulation rate* in other literature.

³ Many countries have well-established networks to monitor airborne particle concentrations in relation to legal standards on ambient air quality. Historically, the main parameter measured was total suspended particulates (TSP), which includes all airborne particles (typically 0–40 μm). More recently, regulatory standards are based on PM_{10} (the concentration in $\mu\text{g m}^{-3}$ of particles with a diameter of 10 μm or less), and $\text{PM}_{2.5}$, with the latter being considered of greater relevance to public health (WHO 2013). Air quality monitoring networks have been used to track volcanic ash plumes (Elliot et al. 2010; Leonard et al. 2014).

⁴ Ash particles released from an umbrella cloud accelerate downward until the air drag retarding them is balanced by their gravitational weight, at which point they reach a steady final speed, or *terminal fall velocity* (Parfitt and Wilson 2009; Rose and Durant 2009).

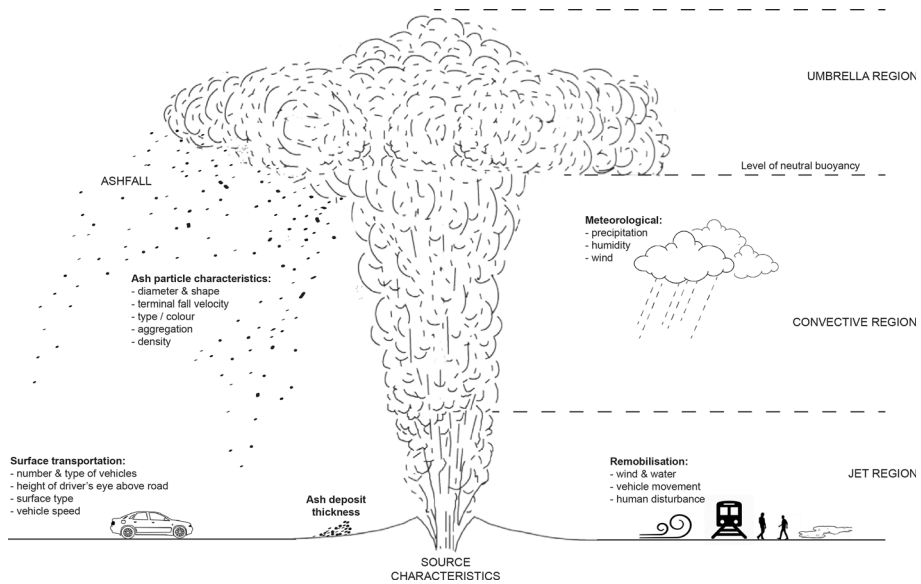


Fig. 1 Eruption and environmental characteristics that influence volcanic ash-settling rates and airborne concentrations (eruption column characteristics modified from Sparks 1986; Carey and Bursik 2015)

particle size, there are somewhat limited primary empirical data available for volcanic ash-settling rates obtained from field measurements or indeed from records of ashfall duration associated with ash thickness or loading in the field. Mean settling rates can be estimated based on the total ashfall duration (e.g. see: Hill 2014), although it is possible that pulses of ashfall with periods of quiescence occur during that time (Scasso et al. 1994). Furthermore, complications from plume and atmospheric turbulence, particle–particle interaction and atmospheric conditions (Bonadonna et al. 2011) mean that accurate correlations between total ash thicknesses and settling rates are difficult to produce.

2.3 Particle size

Unlike airborne mineral dust, which often has a homogeneous internal structure consisting of similar-sized particles, volcanic ash is generally inhomogeneous; the size of erupted material may vary by several orders of magnitude (Weinzierl et al. 2012). However, the most important volcanic ash particle size range in terms of impact to infrastructure including transportation is generally fine-grained ash (e.g. Wilson et al. 2012a; Blake et al. 2016b) (i.e. often < 100 μm diameter, and particularly < 64 μm diameter; Carey and Sigurdsson 1982). Fine ash can disperse for up to hundreds of kilometres from the vent before settling due to gravity and therefore generally settles over extensive areas. The proportions of ash in these fine fractions increase with increasing eruption explosivity (Moen 1981; Horwell 2007; Durant et al. 2009; White et al. 2011), and fine ash is more susceptible to remobilisation by the processes described in point 2 above (Wilson et al. 2011). Particle size distributions of volcanic deposits are poorly constrained due to sparse data, variations in wind conditions and dimensions of eruption columns, and inconsistencies in the methods of measurement. Many particle size analyses carried out for ash deposits are incomplete, lacking data below 63 μm (Bonadonna and Houghton 2005).

2.4 Particle shape

The less spherical a particle shape of the same weight, the lower its settling rate (Komar and Reimers 1978; Wilson and Huang 1979). Volcanic ash particles are often more elongated in shape than other particulates such as mineral dust. Wilson and Huang (1979) found that for volcanic particles of 30–500 μm diameter, glass and feldspar fragments have a very high proportion of flattened particles, whereas pumice consists of a greater variety of shapes (Fagents et al. 2013). More recently, Weinzierl et al. (2012) compared the physical properties of volcanic ash and mineral dust by using samples from Eyjafjallajökull Volcano, Iceland, and the Sahara Desert. The median aspect ratio (i.e. ratio of the width to the height) of Eyjafjallajökull ash was 2.0, compared to a median aspect ratio of 1.6 for the mineral dust. Therefore, because of the general absence of sphericity, settling rates of volcanic ash may be slower than expected on the basis of particle size and weight.

2.5 Measurement of visibility

Visibility involves human perception of the environment, and thus, no instrument truly measures visibility (Malm 1979). Aerosols in the atmosphere, including volcanic ash, interact with light waves leading to absorption and scattering. The amount of light energy redirected from its original path is referred to as the extinction coefficient (b_{ext}) and is equal to the sum of four interactions (Robinson 1968; Hyslop 2009):

$$b_{\text{ext}} = b_{\text{scat,p}} + b_{\text{scat,g}} + b_{\text{abs,p}} + b_{\text{abs,g}} \quad (1)$$

where $b_{\text{scat,p}}$ is the light scattering by particles, $b_{\text{scat,g}}$ is that by gases, $b_{\text{abs,p}}$ is the light absorption by particles, and $b_{\text{abs,g}}$ is that by gases.

The extinction coefficient is thus the optical parameter which is the best proxy for visibility assessment. Once the extinction coefficient is calculated, the corresponding visual range (VR) in metres can be estimated, defined as the longest distance that a large, black object can be seen against the sky at the horizon with the unaided eye (Binkowski et al. 2002; Seinfeld and Pandis 2006; Hyslop 2009; Blake et al. 2016a):

$$\text{VR} = 3.912/(b_{\text{ext}}) \quad (2)$$

where the value at the numerator is constant.

Further information on the extinction coefficient and visual range can be found in Online Resource 1.

Particles smaller than the wavelength of visible light (particle diameter $< 0.05 \mu\text{m}$ in white light) have little effect on visual range. Larger particles (particle diameter $> 2 \mu\text{m}$ in white light), however, have a much greater effect with characteristics such as size, shape and composition being much more influential (Conner 1974; EPA 2000). Although some studies assess the optical properties of volcanic ash at high altitude using remote sensing techniques for the purposes of flying aircraft operability (e.g. Weinzierl et al. 2012), to the best of our knowledge, there have been no detailed quantitative studies of visual range during ashfall near ground level. However, if visibility characteristics associated with volcanic ash can be quantified near the ground, then comparisons with other, more studied atmospheric hazards such as fog and dust storms can be made, and impacts on surface transportation and vehicle mobility estimated. We suggest that where visibility in volcanic ash has not been quantified, precise comparisons to visibility during other atmospheric

hazards cannot be made as the characteristics of certain particles and subsequent effect on light attenuation may be different.

2.6 Effects of visibility degradation on surface transportation networks

Through the common effect of visibility degradation, many atmospheric hazards produce similar consequences for surface transportation. Specifically, previous studies document that the presence of thick fog, smoke or dust influences roads by: (1) reducing the volume of traffic; and (2) increasing the risk of accidents despite lower traffic volumes and an overall reduction in speed—particularly accidents that involve multiple vehicles and cause a higher percentage of severe injuries (OECD 1986; Musk 1991; Ashley et al. 2015; Hardy 2015; Ibrahim 2015).

There have been many studies into the impacts of fog and mineral dust on visibility (e.g. Codling 1971; Moore and Cooper 1972; Hagen and Skidmore 1977; Summer et al. 1977; Perry 1981; Musk 1991; Taylor and Moogan 2010; Abdel-Aty et al. 2011; Weinzierl et al. 2012; USDOT 2013; Ashley et al. 2015). High concentrations of fog droplets and/or mineral dust particulates are required to cause low visibilities and disrupt transportation networks. For example, Hagen and Skidmore (1977) highlight that mineral dust concentrations exceeding 50 to 100 mg m⁻³ seriously reduce visibility during daylight, with lower concentrations hazardous at night. Other atmospheric hazards including smoke from wildfires and airborne volcanic ash, routinely disrupt road networks and inhibit operations at airports, and accidents have been attributed to volcanic ashfall (e.g. Bartney 1980; Folch et al. 2014; Blake et al. 2015). However, they remain relatively under-researched hazards in transportation studies (Cova and Conger 2003, Abdel-Aty et al. 2011).

A recent study by Brooks et al. (2011) used a driver-simulation method to determine how drivers react when driving in varying levels of fog and to assess whether drivers are willing to drive at speeds where their lane-keeping performance is degraded due to the reduced visibility. Observed speed reductions were as follows:

- For visual ranges of 496–31 m, average speeds decreased from 91.3 to 89.1 km h⁻¹
- For 18 m visual range, speeds decreased further to 82.9 km h⁻¹
- In the foggiest condition tested (6 m visual range) speeds decreased to 71.7 km h⁻¹, representing a decrease of ~ 20 km h⁻¹ from clear conditions.

Despite the speed reductions for the most reduced visibility however, it was calculated that drivers would likely be incapable of stopping to avoid obstacles in the roadway (Brooks et al. 2011; Blake et al. 2016a), a situation that corresponds to what has been recorded on actual roads in inclement weather (Edwards 1999). Additionally, lane-keeping ability was reduced when fog resulted in visibility distances < 30 m (Brooks et al. 2011). Mueller and Trick (2012) also used a driver-simulation method to investigate average speeds in fog (with 600 m visual range) and found that all drivers reduced their speed in fog compared to clear conditions, with an average speed reduction of 6.4 km h⁻¹.

Mitigation measures available for managing reduced visibility due to airborne volcanic ash include reducing vehicle speeds (including the implementation of lower-than-usual speed limits); restricting the number and/or type of vehicles on the network; increasing the space between moving vehicles; dampening surfaces with water to minimise the resuspension of ash, and closing roads in especially contaminated areas (Table 1). The only complete solution is the total removal of ash deposits, but this may not be possible or cost-effective.

2.7 Auckland case study

We use Auckland as a case study location to apply our methodology due to the relatively large population (~ 1.6 million people, Statistics New Zealand 2015), extensive transport networks and exposure to multiple sources and types of volcanic ash (Fig. 2).

Basaltic ash may originate from new eruptions in the Auckland Volcanic Field (AVF), on which the city is built, or potentially from Whangarei and Bay of Island volcanic fields to the north (Smith and Allen 1993). Andesite can be deposited from eruptions within the Tongariro Volcanic Centre, located in the Taupo Volcanic Zone (TVZ) and from Taranaki Volcano. Rhyolite may be deposited in Auckland from eruptions within the Taupo and Okataina Volcanic Centres of the TVZ with rhyolitic ash from Mayor Island also possible. Recent work by Zawalna-Geer (2016) suggests that Auckland has been inundated by tephra at least once every 424 years on average. However, any recurrence rates must be considered with caution due to different climatic regimes and because not all eruptions will be preserved in the geologic ash record, and certainly not all eruptions will be represented by ash at specific coring sites (Lindsay and Peace 2005). Auckland is exposed to ashfall with a relatively wide range of airborne concentrations, settling rates, as well as particle sizes, densities and shapes (Smith and Allen 1993). As such, many of the methods and results in this paper are internationally applicable.

Visual range for excellent conditions is typically taken to be > 70 km (MFE 2001). Indeed, the mean visual range taken over a three year period (from 2001 to 2003) from readings over Auckland City (Dr Gerda Kuschel, Auckland Council, pers comm, 21 June 2016) is similar, calculated at 66.5 km with 95% CI [65.1, 67.8]; the shorter visual range is unsurprising given the city environment with likely higher background particulate concentrations than “typical excellent” conditions.

3 Methodology

Our methodology outlines the novel technique used to simulate ashfall and to simultaneously measure ash-settling rates and extinction coefficients (subsequently used to calculate visual ranges using Eq. 2) in a laboratory environment. Visual ranges through ashfalls of different particle sizes and types and settling rates, representing those considered possible in Auckland, may thus be determined.

3.1 Experimental set-up

The key equipment used for our experimental set-up is a transmissometer to calculate visual range, and solid aerosol generator to disperse ash, both selected specifically for the purpose and incorporated into a custom-made experimental set-up.

3.1.1 Transmissometer

We use a dual-pass transmissometer (DynOptic DSL-460 MkII) for our experiments. The transmissometer is adopted to measure the optical characteristics over a preset path length of 1.4 m. It measures a specific amount of green light transmitted from the source/-transceiver securely mounted to the side of a container, to a reflector mounted opposite and back to the same transceiver (Fig. 3). This allows the direct and continuous (1 s interval)

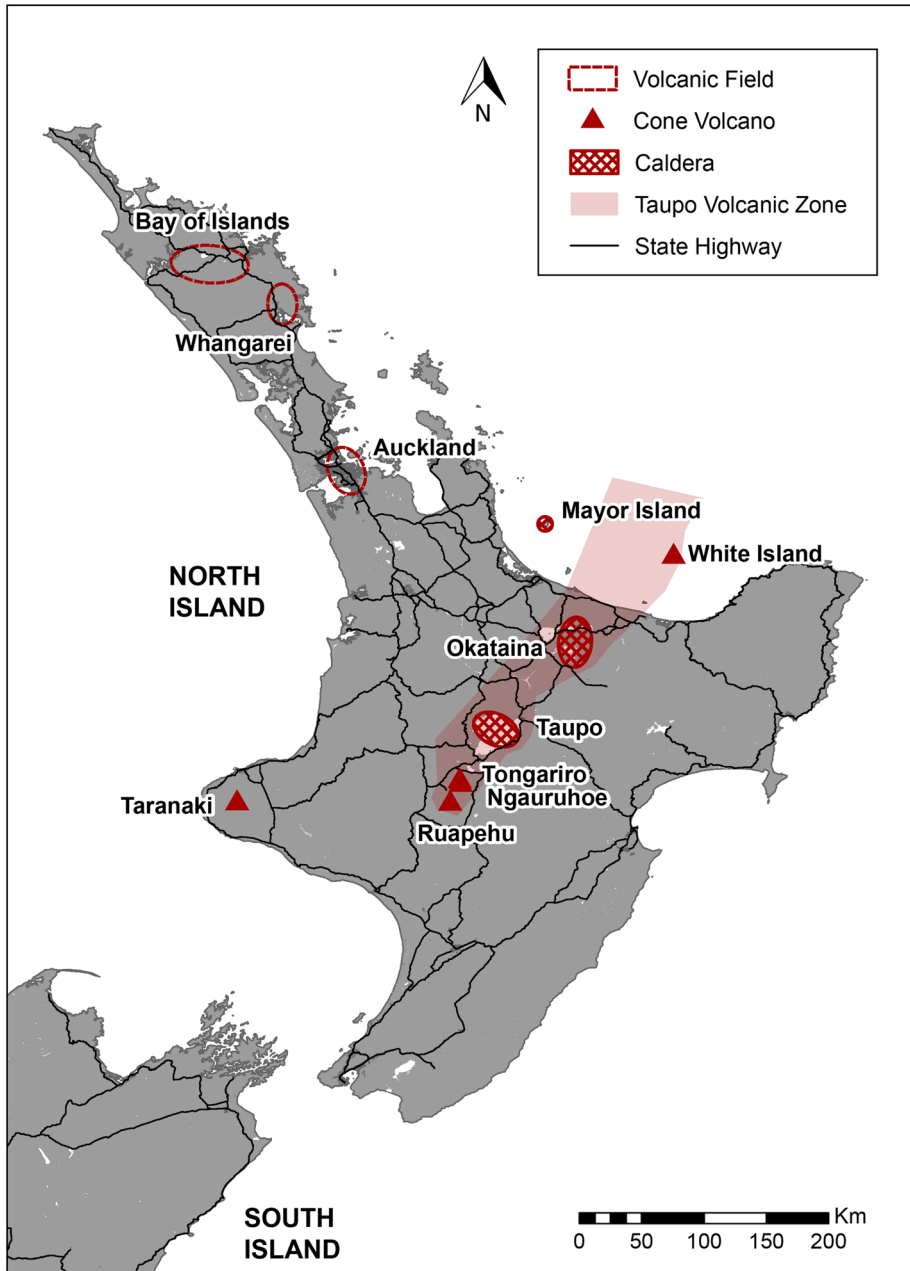


Fig. 2 Potential sources of volcanic ash in New Zealand that could affect Auckland

calculation of the extinction coefficient of the air along the path length for light with a wavelength at which the human eye observes. A small amount of ash accumulates on the optics of the transmissometer during each test. However, following trial tests, this was substantially limited by extracting purge air (which the instrument uses to clean the optics

during operation) through ducting from an adjacent clean room. Following the extraction of purge air from a clean source, the accumulation of ash on the optics accounted for only $\sim 1.0 \times 10^{-6}\%$ of the maximum values recorded which is deemed insufficient to substantially affect findings. The transceiver and reflector are simply cleaned with

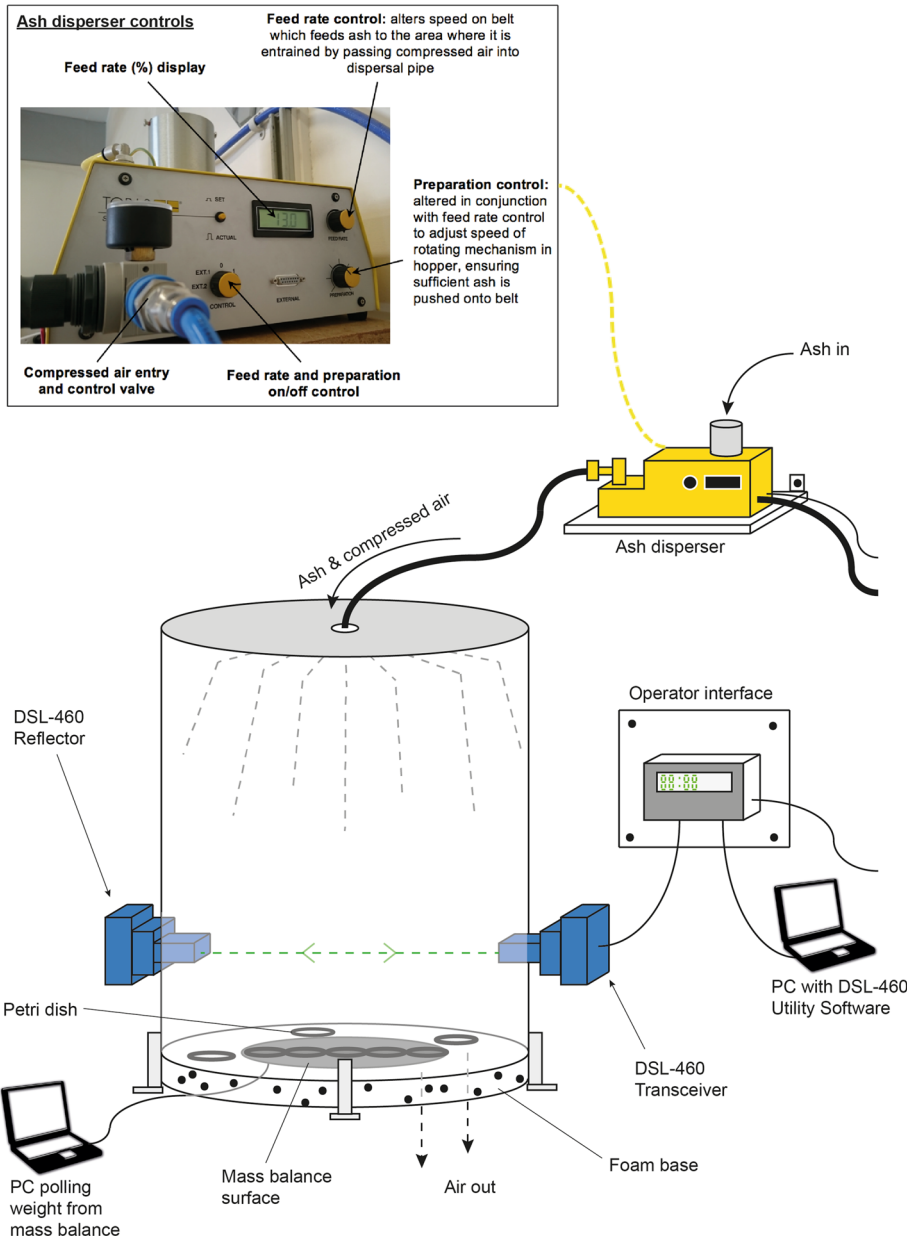


Fig. 3 Experimental set-up developed and implemented for visibility testing (adapted from Blake et al. 2016a)

compressed air between each experiment and results corrected so as to always start with zero values for the extinction coefficient and avoid drift. We refer the reader to Online Resource 2 for further information on transmissometers, and to the DynOptic DSL-460 MkII operation manual (DynOptic 2014) for detailed information on the calibration and operation procedures for this particular transmissometer.

3.1.2 Ash disperser

Precise and consistent ash-generation rates (g h^{-1}) are produced using a solid aerosol generator (Topas SAG 410) (named *ash disperser* from herein) into the top and centre of a purpose-built stainless-steel cylindrical container (Fig. 3), shaped as such to encourage evenly distributed flow because trial tests suggested that cylinders were preferential to cuboids where ash-settling rate varied in corners.

Two simultaneous methods for calibration of the ash disperser for each ash type of particular particle diameter size distribution were used to determine the machine settings required for different generation rates and estimated ash-settling rates in the container; a gain-in-weight technique where ash dispersed from the instrument is collected in filter bags and weighed, and a loss-in-weight technique where the whole instrument weight is recorded before and after ash dispersal.

3.1.3 Ash-settling rate measurement

When the ash enters the container, a purpose-built nozzle on the end of the tube causes the ash to be dispersed in all directions before settling under gravity. The height of the container (1.3 m total, with a 1 m fall distance to the light beam of the transmissometer) was chosen by considering formulas derived from Bonadonna et al. (1998), which suggest that the majority of ash particles dispersed reach terminal velocity before passing through the measurement level. However, the set-up was also constrained by workspace limitations and accessibility requirements to the hopper of the ash disperser, which had to be positioned above. Beneath the measurement level of the transmissometer, the ash settles at the base of the container (0.75 m^2 in area). Half of the area (i.e. 0.375 m^2) at the centre of the base is dedicated to a circular board on top of an automated mass balance set to poll and record the weight of ash every 10 s. The other half around the edge consists of foam, which allows the air to evenly escape from the base of the container and the vast majority of ash to remain static when out of suspension. Trial tests suggested that the solid board at the centre had little influence on ash flow currents towards the base of the container and that there was minimal remobilisation of ash that would affect results.

Some radial differences in ash-settling rates were identified for samples, both for individual experiments and between experiments. However, the consistent airflow within the container, along with the light beam traversing the entire diameter, means that there is negligible effect on the transmissometer readings and that the entire horizontal transect would appropriately represent a steady ashfall. To account for the radial differences in settled ash at the base (i.e. because the board does not cover the whole area), a series of ten petri dishes are equally positioned (five on the central board and five on the foam edge). These are weighed after each experiment to analyse the distribution profile for the settling ash in our experiments. The results from the petri dishes, in conjunction with the centred mass balance weights, are used to calculate and record mean “actual” (rather than estimated) ash-settling rates ($\text{g m}^{-2} \text{ h}^{-1}$) at the base (Sect. 4.1).

Preliminary test runs revealed that equilibriums between ash generation into the container and ash settling at the base occurred within 15 min for all ash types. Therefore, every experiment for each ash type at a specific generation rate and distribution for particle diameter size is run for a total of 1 h where possible (some high generation rates caused ash supply to be exhausted within 45 min). This allows at least 30 min of continuous measurement at equilibrium conditions, which is sufficient time for a mean value of the extinction coefficient and visual range for each sample and ash-generation rate to be calculated. The transmissometer is then left operating for at least a further 15 min after the disperser is switched off to allow continued monitoring, whilst all the ash settles out. Ash is cleaned from the board, foam and container edges between each experiment and a thorough clean of all equipment is conducted. The ash disperser tube is disposed of and replaced at the end of testing with each ash sample.

3.2 Application to Auckland

Methods used to replicate ash types, particle sizes and settling rates that can be expected in the city given a future volcanic eruption in the AVF or from the larger volcanoes of the central North Island of New Zealand are described in Sects. 3.2.1–3.2.3, respectively.

3.2.1 Ash type

Basaltic, andesitic and rhyolitic ashfall is possible in Auckland, and we conduct experiments with all three types; a dark-coloured basalt which is sourced from a deposit of Pupuke Volcano in the AVF, a mid-coloured andesite derived from a deposit from the Poutu eruption of Tongariro Volcano, and a light-coloured rhyolite from the Kaharoa eruption of Tarawera Volcano, in New Zealand (Table 2). The raw samples were largely selected from sources outside of the AVF, as many of those within the AVF have been weathered, contaminated by organic material and/or disturbed or removed by human activity (e.g. Alloway et al. 2004; Cassidy and Locke 2004; Howe et al. 2011; Adams 2013). Our samples were modified through pulverisation to achieve a range of particle diameter size distributions possible in Auckland and thus likely contain a higher than natural proportion of particles that are blocky in nature with a high degree of angularity due to the milling process (Broom 2010). Therefore, an additional fine-grained sample (sourced from the 2008 eruption of Chaitén in Chile—Table 2) is also tested to investigate the effects of particle shape on visual range. This sample was not altered through pulverisation and only sieved to remove the larger particles that can cause clogging of the ash disperser. All samples were dried at 65 °C for > 48 h prior to testing.

3.2.2 Particle size

Following a detailed literature review, we further developed work by Hill (2014) to estimate ash particle sizes that can be expected in Auckland from volcanic sources in New Zealand (Fig. 4). Unlike Hill (2014) however, who focussed solely on median data, we incorporate all available data for particle size, including individual data or median size recorded at specific locations from a vent (shown as points in Fig. 4), modes (bold points or bold ranges), full distributions (vertical “error bars”) and distributions in spatial extent (horizontal “error bars”). Triangles in Fig. 4 denote maximum clast sizes of blocks, and black data points show particle sizes and distances from vents determined from recent

Table 2 Characteristics of the four ash types used for experimentation

	Pupuke, Auckland Volcanic Field, New Zealand	Poutu, Tongariro, New Zealand	Kaharoa, Tarawera, New Zealand	Chaitén, Chile
Year of eruption	~ 200,000 BP (Leonard et al. 2017)	~ 11,000–12,000 BP (Hitchcock and Cole 2007)	1314 (Sahetapy-Engel et al. 2014)	2008 (Lara 2009)
Ash type	Basalt	Andesite	Rhyolite	Rhyolite
Colour (determined from Munsell Rock Colour Chart)	N4: medium dark grey	5Y 6/1: light olive grey	5YR 5/2: pale brown	5Y 8/1: yellowish grey
SiO ₂ content (determined by Philips PW2400 XRF analysis)	44% (mafic)	52% (intermediate)	75% (felsic)	75% (felsic)
Dominant minerals (determined by Philips XRD analysis)	Diopside, Forsterite, Anorthite	Albite, Augite	Albite, Quartz	Albite
Particle size group	a b c	b	b	b
Mode particle size (µm) (see Fig. 5)	12 45 105	22	30	21
Dry bulk density (g cm ⁻³)	0.92 1.12 1.28	0.89	0.87	0.83

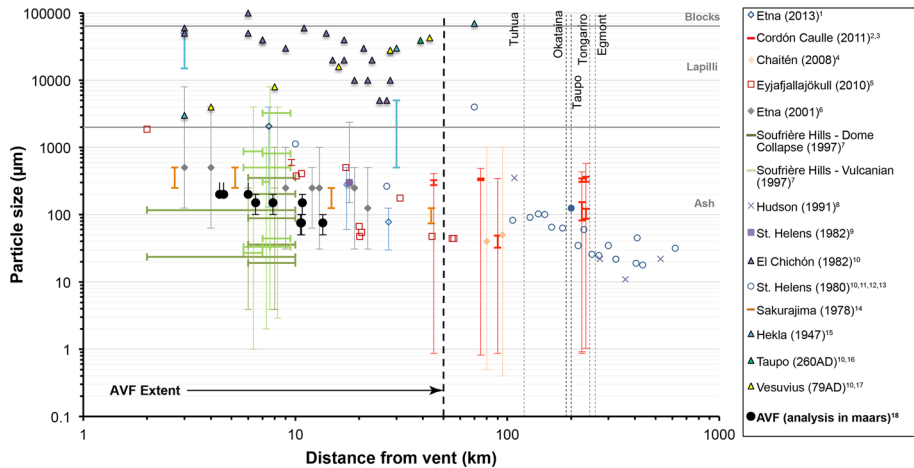


Fig. 4 Particle sizes of ash deposits and their associated distances from 15 worldwide eruptive vents and analysis from maars in the AVF. The distances from central Auckland (depicted as 0 km) to New Zealand volcanic ash sources are identified by a series of dashed vertical lines, and approximate maximum axial extent of the AVF by a bold dashed vertical line. Solid horizontal grey lines denote the boundaries between ash and lapilli (2 mm) and lapilli and block (64 mm) particle diameters. Data from: ¹Andò et al. (2014), ²Wilson et al. (2013), ³Heather Craig, University of Canterbury, pers comm, 17 July 2014, ⁴Watt et al. (2009), ⁵Bonadonna et al. (2011), ⁶Scollo et al. (2007), ⁷Bonadonna et al. (2002), ⁸Scasso et al. (1994), ⁹Harris and Rose (1983), ¹⁰Carey and Sigurdsson (1986), ¹¹Scheidegger and Federman (1982), ¹²Sarna-Wojcicki et al. (1981), ¹³Carey and Sigurdsson (1982), ¹⁴Eto (2001), ¹⁵Wilcox (1959), ¹⁶Walker (1981), ¹⁷Sigurdsson et al. (1985), ¹⁸Jenni Hopkins, Victoria University of Wellington, pers comm, 19 July 2014

analysis of deposits in six Auckland maars from historical AVF eruptions of One Tree Hill, Three Kings and Mt Eden Volcanoes (Jenni Hopkins, Victoria University of Wellington, pers comm, 19 July 2014).

Due to the maximum particle size constraints of the ash disperser and likely clogging when particle diameters exceed $\sim 300 \mu\text{m}$, our experiments focus on samples defined as *fine ash* by Carey and Sigurdsson (1982) and Folch et al. (2009), in that mode particle diameters for most samples are $< 64 \mu\text{m}$. All mode particle diameters are $< 110 \mu\text{m}$ (Fig. 5). However, we subdivide our samples into three categories of mode particle diameter size for ease of interpretation; a. $< 20 \mu\text{m}$, b. $20\text{--}50 \mu\text{m}$ and c. $> 50 \mu\text{m}$ (Table 2). For the basalt sample, we test ash for all three categories to investigate the effect of particle diameter size on visual range. For the andesite and rhyolite samples however, we only test for the category b range due to ash sample availability. Specific ash particle sizes were achieved using a rock pulveriser with different disc separation distance and sieves with different mesh aperture sizes, followed by laser sizing to determine the particle diameter size distributions. Total particle diameters for all samples used are $\sim 1\text{--}320 \mu\text{m}$ (Fig. 5) which corresponds with the mid- to lower-grain sizes of ash particles that can be expected in Auckland given a future eruption in New Zealand (Fig. 4).

3.2.3 Estimated ash-settling rates

As the generation rate of each ash type and particle size is determined as part of the instrument calibration, estimations of settling rate can be made given the known volume of the container where the ash is dispersed and replicated under controlled conditions. As with

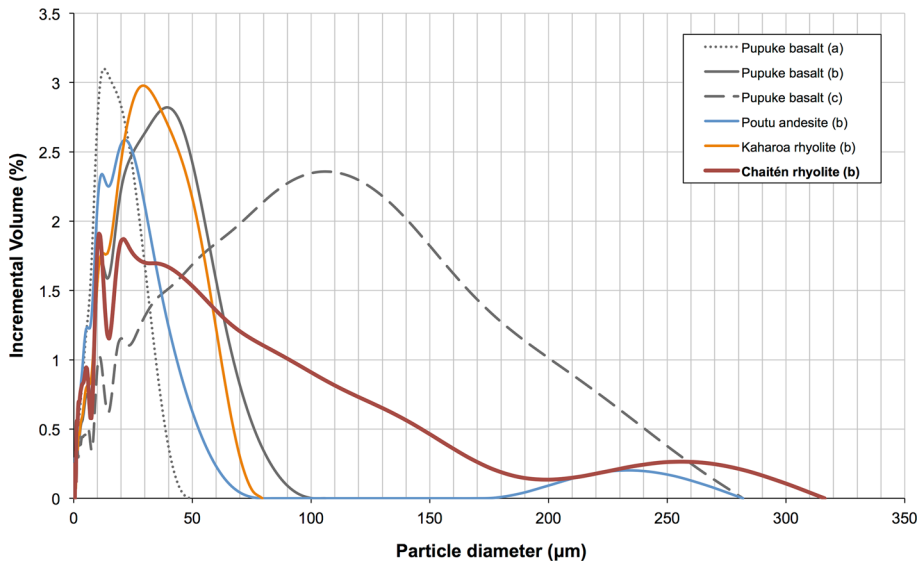


Fig. 5 Particle diameter size distribution plots for the ash used in experimentation, derived from three tests per sample using a Micromeritics Saturn DigiSizer II laser size instrument. **a–c** refer to the mode size categories shown in Table 2. All ash samples used generally have a normal distribution for particle sizes, with the exception of the rhyolite sample from Chaitén, where particle sizes have a distinctive positive skew

particle sizes, all available worldwide ash-settling rate data were plotted, which showed a generally decreasing settling rate with distance from vent (Fig. 6).

Based on the settling rates in Fig. 6, and the particle sizes adopted for experimentation (Table 2), which represent ashfall in Auckland from distal eruptions or mid- to lower-particle sizes expected from an AVF eruption, we attempt to replicate ash-settling rates between 50 and $1000 \text{ g m}^{-2} \text{ h}^{-1}$ (four specific ash-settling rates within this range per sample) for all six of the samples. However, we also attempt to replicate settling rates towards the upper limit of what can be expected in Auckland (i.e. around 2000 and $10,000 \text{ g m}^{-2} \text{ h}^{-1}$) for the Pupuke basalt and Chaitén rhyolite (category b) samples, where more material was available, to determine expected absolute minimum visual ranges from direct ashfall in the AVF. Thus, in addition to multiple trial tests, a total of 28 experiments are conducted as part of this study.

We highlight that the ash-settling rates determined at this stage are those forecast using the ash disperser calibration results. Actual ash-settling rates at the base of the container are lower; particularly for high ash-generation conditions, due to:

- Adherence of some ash to the container side and top reducing the airborne concentration and settling rate.
- An increase in pressure within the container acting against more ash entering as compressed air continues to enter at the top of the container, but the foam at the base becomes clogged.
- Leakage of some ash from the container altogether, either through the foam or small gaps, especially when the air pressure inside is very high.

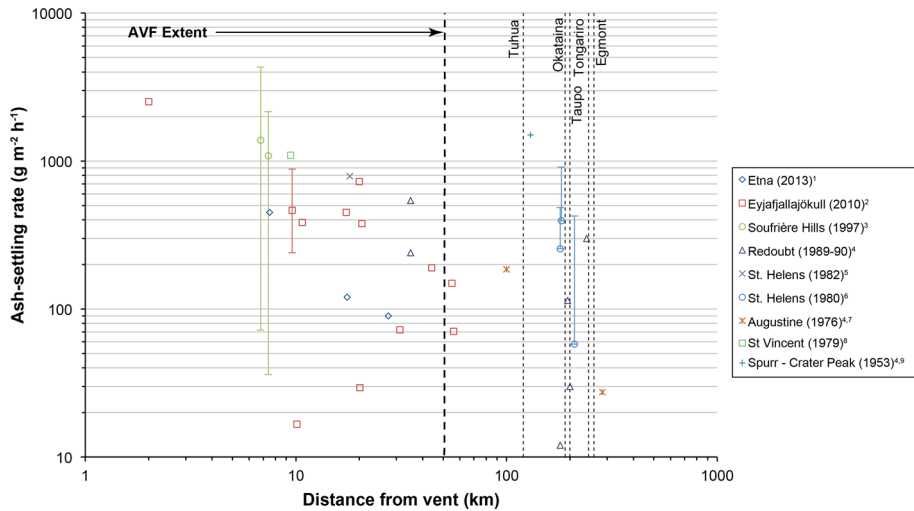


Fig. 6 Ash-settling rates and their associated distances from nine worldwide eruptive vents. The distances from central Auckland (depicted as 0 km) to New Zealand volcanic ash sources are identified by a series of dashed vertical lines, and approximate maximum axial extent of the AVF by a bold dashed vertical line. Data from: ¹Andò et al. (2014), ²Bonadonna et al. (2011), ³Bonadonna et al. (2002), ⁴Scott and McGimsey (1994), ⁵Harris and Rose (1983), ⁶Scheidegger and Federman (1982), ⁷Kienle and Swanson (1985), ⁸Brazier et al. (1982), ⁹Wilcox (1959). A value of $1100 \text{ g m}^{-2} \text{ s}^{-1}$ was also identified in Self et al. (1974), but the duration of this rate is unclear and it involved scoria material with a predominant particle size of $\sim 6 \text{ mm}$. Therefore, we decided not to extrapolate it to 1 h for the purpose of this chart

Actual ash-settling rates are determined from the centred mass balance and petri dish procedure outlined in Sect. 3.1.3.

4 Results

4.1 Ash concentrations and settling rates

Measurements of airborne ash concentration taken directly from the transmissometer were $\sim 40\text{--}1600 \text{ mg m}^{-3}$ for all experiments, with higher values corresponding to the highest ash-settling rates and lowest visual ranges (Online Resource 3–4). There were no distinct differences between airborne particle concentration reductions for the different ash samples or ash-generation rates we used in experimentation. It took $11 \text{ min} (\pm 2 \text{ min})$ for airborne concentrations to return to original levels. However, given the exponential decay in airborne particle concentration following the cessation of new ash entering the container, values decreased to $< 10\%$ of their maximum values in less than 5 min.

For the relatively coarse-grained ash samples (particularly size category c, and to some extent b), a greater weight of ash and more ash of larger particle size fell towards the centre of the container base, with ash becoming more fine-grained towards the edge. Fine-grained ash adhered to the edge and top of the container (Fig. 7). Adherence was prevalent for the ash samples with the finest particle sizes (i.e. category a, and to some extent b), and especially so for the Chaitén rhyolite sample, causing sometimes large decreases in ash-settling rates towards the extreme edge of the base.

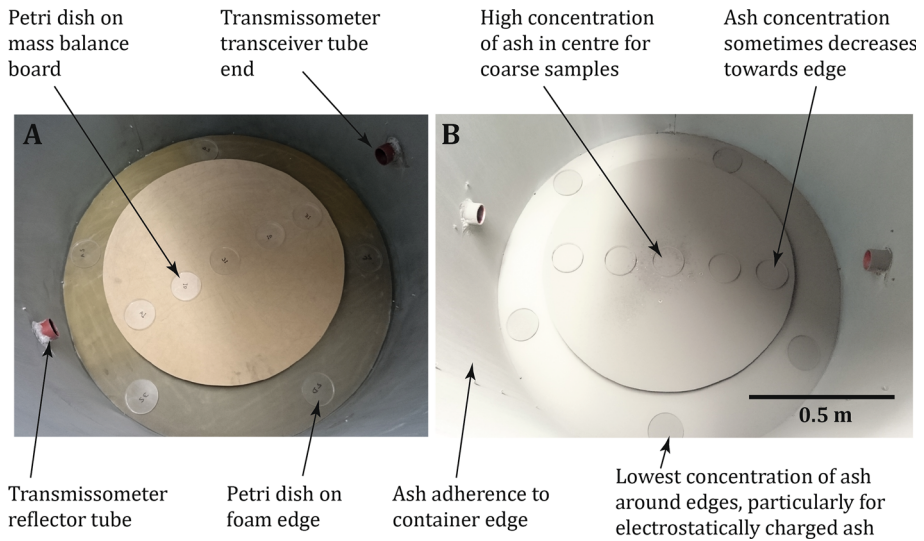


Fig. 7 Annotated plan-view photographs taken looking down into the container showing **a** petri dishes on the central mass balance board and foam edge, and **b** describing general ash accumulation patterns across the container base, determined from the mass of ash on the centred board and in petri dishes, and through visual observations after each experiment

Due to the inconsistencies across the container base, results displayed for ash-settling rates are in the form of three values, corrected for a 1-h period over 1 m^2 :

1. A minimum value calculated from the weight recorded on the centred mass balance board at the container base multiplied by a correction factor determined by the weight difference between ash in the petri dishes on the board and on the foam edges for that particular sample.
2. A maximum value calculated by doubling the weight recorded on the central mass balance board at the container base for that sample to assume the same weight falls on the foam edge.
3. The midpoint between points 1 and 2 above, which is deemed the value most likely to represent the true ash-settling rate.

Based on these values, although ash-settling rates forecast from the ash disperser calibration were $\sim 50\text{--}10,000 \text{ g m}^{-2} \text{ h}^{-1}$ (Sect. 3.2.3), the actual ash-settling rates for our results are calculated at $28\text{--}4800 \text{ g m}^{-2} \text{ h}^{-1}$.

4.2 Visual ranges

Figure 8 shows an example of the direct visual range reading from the transmissometer for one experimental run. In our results, the maximum and minimum values recorded by the transmissometer have greater deviation from the mean for the lowest airborne concentrations and ash-settling rates.

For the Pupuke basalt, which had the highest bulk density of the four ash types used, testing was conducted using three distinct particle diameter size distributions, the results of which are summarised in Fig. 9 with data values in Online Resource 3. It is evident that for a given ash-settling rate, visual range is less for ash predominantly containing finer

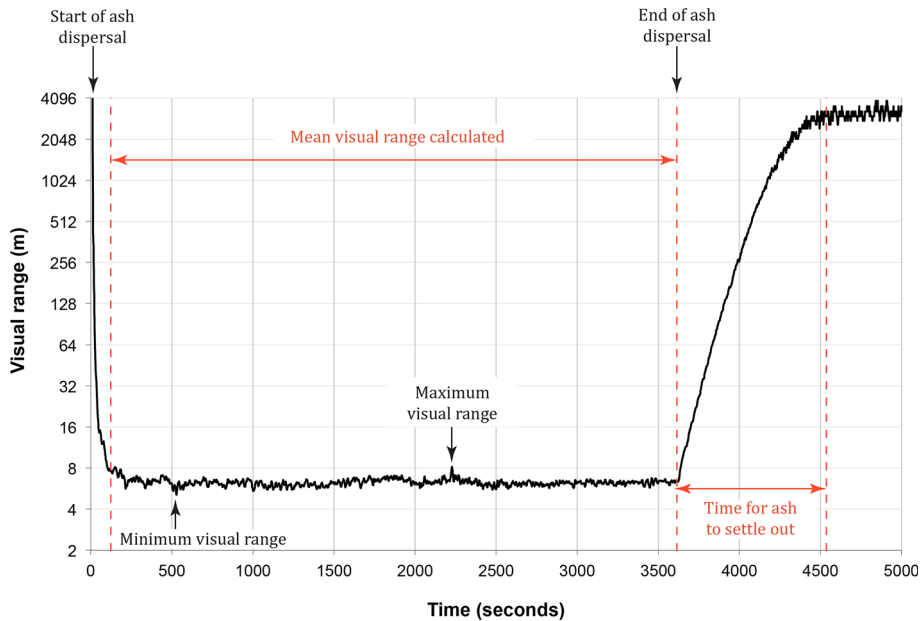


Fig. 8 Unprocessed transmissometer results for the Kaharoa rhyolite sample when ash was dispersed at the highest generation rate tested. Annotations show how the mean, maximum and minimum visual ranges were determined, as well as time taken for all ash to settle out and airborne concentration and visual range to return to original conditions

particles. Lines of best fit follow inverse power relationships (Fig. 9). Similarly, relationships between visual range and ash-settling rates are best described by inverse power law relationships for the rhyolitic and andesitic ash types (Fig. 10 and Online Resource 4 for data values). The Chaitén sample produced results with greater visual ranges than all other types in the same particle size category, despite being the lightest-coloured ash we tested.

5 Discussion

This section includes a discussion of our experimental approach and considerations for visibility in airborne volcanic ash in both a general sense and specifically forecast conditions for Auckland. We then outline key limitations of the approach adopted and recommendations for future adaptations and additions to the methodology. Finally, we consider implications of reduced visibility for transportation operation and provide examples of mitigation strategies that transportation and emergency management officials could implement based on findings from this study and other recent work.

5.1 Visibility in airborne volcanic ash

Our results demonstrate that the new methodology and experimental set-up developed is suitable to produce sufficiently consistent ash-settling rates to analyse visual range through airborne volcanic ash in laboratories. Compared to most other airborne particulate matter,

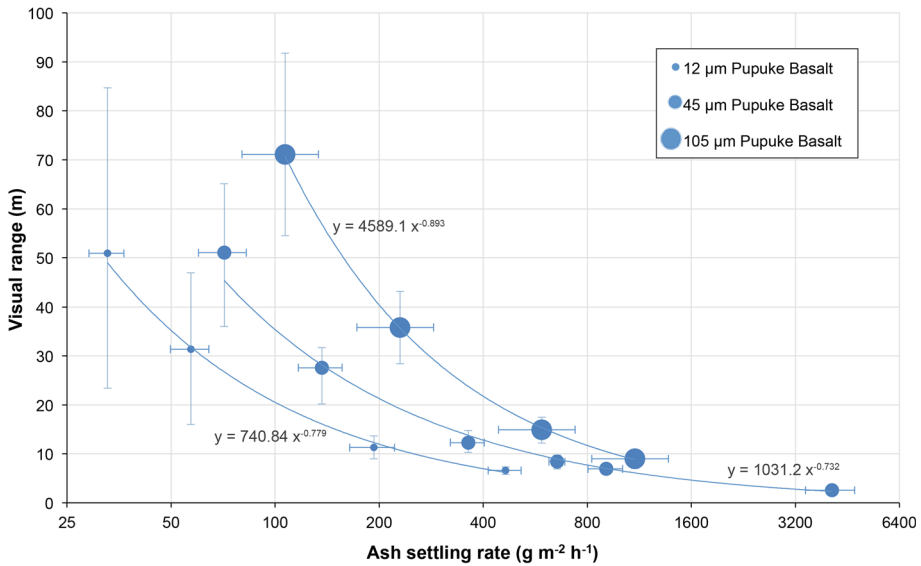


Fig. 9 Visual ranges for the three Pupuke basalt particle diameter size distributions. Each point is for the mean visual range when ash flow into the container was at equilibrium with ash-settling rate at the base for each experiment. Horizontal minimum and maximum error bar values and the point values correspond to bullet points 1–3 in Sect. 4.1, respectively. Vertical error bars show the maximum and minimum values recorded by the transmissometer during the periods of equilibrium (Fig. 8)

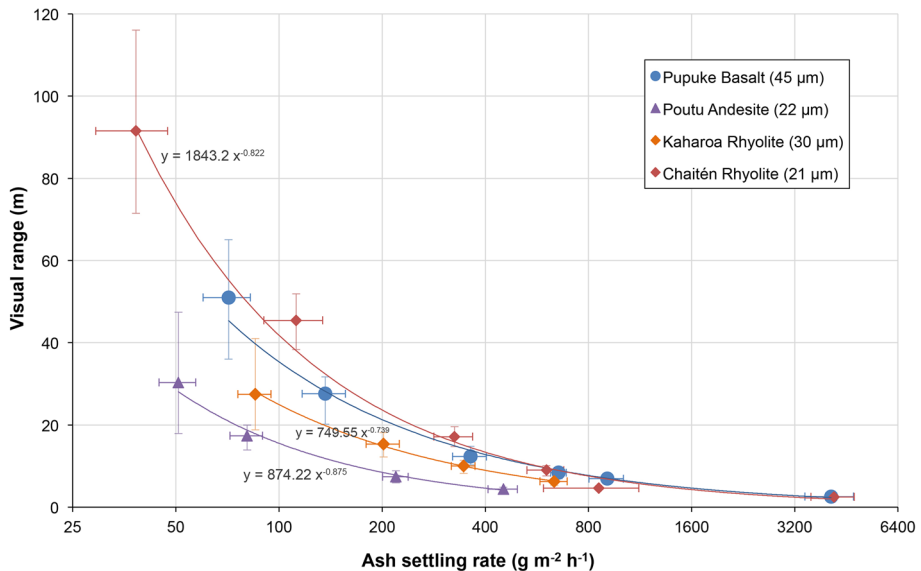


Fig. 10 Visual ranges for the four ash samples in particle diameter size distribution category b (i.e. 20–50 µm mode diameters). Each point is for the mean visual range when ash flow into the container was at equilibrium with ash-settling rate at the base for each experiment. Horizontal minimum and maximum error bar values and the point values correspond to bullet points 1–3 in Sect. 4.1, respectively. Vertical error bars show the maximum and minimum values recorded by the transmissometer during the periods of equilibrium (Fig. 8)

ash particles are relatively large in size. However, their occurrence in large concentrations, like fog droplets, can cause substantial reductions in visibility, although they generally fall to the ground and out of suspension more quickly.

The time taken for the airborne ash concentration to reduce to zero upon cessation of dispersal at the top of the container is of particular interest. It provides an indication of how long remobilised ash would take to settle from a 1 m height above the ground given no ongoing disturbances such as wind or traffic and in the absence of rainfall. This type of information can be used to inform transportation management strategies such as the spacing of rail or road vehicles to allow sufficient time for ash to settle and reduce visual impairment to drivers (Sect. 5.3). Adherence of ash to the container is likely explained by the electrostatic charging of ash particles (Bonadonna and Phillips 2003; Folch 2012). However, as the light beam of the transmissometer passes the width of the container (1.4 m path length) and because inconsistencies occur in a radial pattern, this allowed the accurate calculation of mean ash-settling rates.

Visual range fluctuates between readings (Fig. 8), depending on the quantity and characteristics of particles within the light beam of the transmissometer at the precise time of measurement. However, as values are recorded at one-second intervals and because we calculate each mean visual range result from at least 30 min of experimentation, i.e. > 1800 data points, we consider our results reliable.

The result that visual range is lower for ash containing finer particles corresponds to the findings by Conner (1974), in that the mass scattering efficiency of light decreases as particle size increases. Comparing the Pupuke basalt and Kaharoa rhyolite, which were pulverised and sieved with the same dimension controls, results suggest that the light-coloured rhyolite causes lower visual ranges than the dark-coloured basalt. This makes intuitive sense, as there is more reflection from light-coloured surfaces. Low visual ranges for the andesite sample are perhaps explained by augite being one of the dominant minerals (constituting ~ 20% of the sample). With two prominent cleavages, meeting at angles near 90 degrees for augite, light scattering may be relatively high. Furthermore, the particle sizes for the andesitic ash are low compared to the basalt and Kaharoa rhyolite, and fallout of the andesite may be slowed by relatively irregular particle shapes (Riley et al. 2003; Pardini et al. 2016).

The most likely explanation for the unexpected visual range results obtained for the Chaitén sample is due to the larger positive particle size distribution from the mode than the other samples (Fig. 5), and thus higher proportion of relatively large diameter particles. Additionally, the comparatively low processing undertaken when producing this sample led to particles that are relatively spherical in shape (Fig. 11). As such, they reflect less light than the irregular-shaped particles of the other samples we tested. In fact, the Chaitén ash is more representative of fresh volcanic ash samples and our results for the other samples, which were all mechanically pulverised, thus provide a worst-case situation for visual range reduction during initial ashfall in this regard.

5.1.1 Consequences of ashfall events in Auckland for visibility

Our results sufficiently cover the range of settling rates that can be expected in Auckland given a future eruption in New Zealand based on correlation with the limited dataset available from worldwide eruptions (Fig. 6). Ash-settling rates of ~ 1000 g m⁻² h⁻¹, possibly up to ~ 4000 g m⁻² h⁻¹, may occur in Auckland from any of these eruption locations (Fig. 6), and extrapolation of the line of best fit for the finest grained ash we

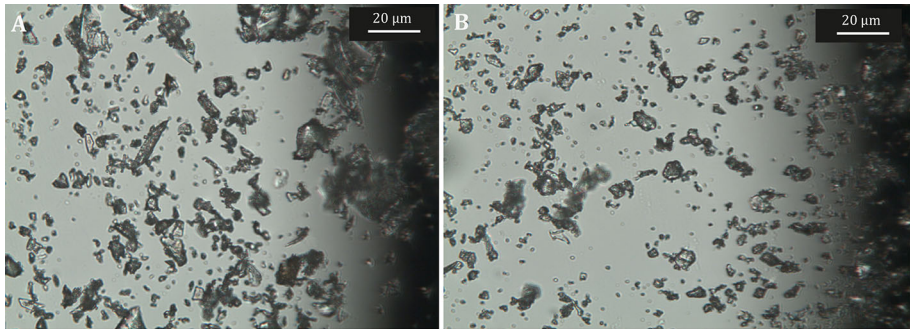


Fig. 11 Microscope images for **a** Kaharoa rhyolite sample, **b** Chaitén rhyolite sample, both in particle size group b. The individual particles of the Chaitén sample are generally more spherical in shape. A Leica DM2500P microscope (with $\times 40$ zoom) and Leica DFC295 camera attachment was used to capture the images

tested (12 μm mode particle diameter) to these settling rates suggest that visual ranges as low as $\sim 1\text{--}2$ m can occur under such conditions.

Ash-settling rates are likely to be higher (resulting in shorter visual ranges) nearer to the vent and for explosive eruptions, which generally produce a relatively large proportion of fine-grained ash (White et al. 2011). For Auckland, small ash particle diameter sizes are possible from eruptions in both the AVF and TVZ of New Zealand (given appropriate wind directions). However, even the smallest estimated ash-settling rates in Auckland ($\sim 10 \text{ g m}^{-2} \text{ h}^{-1}$) during an eruption would cause a visibility reduction of over two hundred times from typical baseline visual range (i.e. < 300 m rather than 70 km visual ranges) for ash with characteristics in the range we tested.

5.2 Key limitations and suggestions for future work

- Accurate source data for ash-settling rates (and particle concentrations) following past eruptions are somewhat limited, and forecasts remain constrained by the small dataset. We anticipate that the recent development of automated ash sampling instrumentation (e.g. Shimano et al. 2013; Weber et al. 2013, Andò et al. 2014; Tajima et al. 2015) and their deployment during and following future eruptions will improve understanding of settling rates and reduce uncertainty.
- All of our experiments incorporated only fine-grained ash (all particle diameters $< 320 \mu\text{m}$ with mode sizes $< 110 \mu\text{m}$) due to limitations of the ash dispersal equipment which was prone to clogging by coarse particles. However, the particle size distributions of our ash samples are generally polydisperse and appropriately replicate fine-grained ashfall that could occur in Auckland from diverse sources.
- All ash samples were oven-dried to obtain consistent dryness prior to investigating particle characteristics. Therefore, we have not accounted for relative humidity affecting the ash over time, although the ash was exposed to relatively stable humidity in the laboratory when conducting the experiments. Visibility in mineral dust storms is known to decrease if the relative humidity is high, particularly if more than 70% (Hagen and Skidmore 1977). We speculate that if volcanic ash encounters higher relative humidity, there will likely be greater light scattering and lower visual range due

to the hygroscopic properties that the particles exhibit (Malm et al. 2003; Barsotti et al. 2010). Therefore, Eq. 2 may underestimate visibility reduction.

- Although the transmissometer records regular measurements of airborne particle concentration, we view these data with caution in this study, as precise values would require the density correction factor (set as 1.00 for our tests) to be adjusted between each sample. In the absence of complex isokinetic sampling of the airborne ash in the container, this cannot be achieved (DynOptic 2014), and we recommend this addition for future work. However, we adopted ash-settling rate as an alternative unit of measurement, which avoided the need for isokinetic sampling processes in our study.
- It was evident that the Chaitén sample became highly electrostatically charged with many discharges occurring when touching the container both during experimentation and subsequent cleaning. More specifically, we suggest that the process of triboelectrification, described in relation to volcanic ash by Aplin et al. (2014) and Aplin et al. (2015), occurred frequently for the Chaitén sample. Triboelectrification is the type of contact electrification that occurs when two materials make contact with each other; Some electrical charge transfers from one material to the other with one gaining and the other losing electrons (Electrostatic Solutions Ltd. 2000). This process can occur readily in volcanic ash with a polydisperse particle size distribution dominated by very fine particle sizes (Aplin et al. 2014), such as our Chaitén sample (Fig. 5). If charged particles are physically separated, charges dissipate to earth, generating sudden electrostatic discharges. Additional testing using further samples is required to confirm this hypothesis and appropriately account for these electrostatic properties.
- Given that ash deposits are often characterised across transects or accessible lines rather than across grids (Folch 2012), and given the number and complexity of variables associated with the remobilisation and resuspension of ash (e.g. meteorological conditions, ash wetness, particle characteristics, road surface specifics and vehicle type), we do not investigate the conditions for resuspended ash in detail. Rather, our calculations of visibility impairment largely represent conditions that can be expected during initial ashfall when ash accumulation on the ground is minimal. Current developments in resuspension modelling (e.g. Folch et al. 2014; Reckziegel et al. 2016; Miwa et al. 2018) will aid the future understanding of interactions between ash remobilisation and visibility effects. Our results are presently most reliable for road transportation where ground surfaces are wet and for maritime transportation, as atmospheric remobilisation will be minimal under these conditions. For ongoing eruptions however, our results should be treated as highly conservative for most land-based transportation types where cleaning has not occurred.

5.3 Considerations for transportation

From recent studies that examine impacts on road transportation from visibility degradation caused by fog (Sect. 2.6), we make comparisons to our experimental findings for airborne ash. It is evident that even the lowest ash-settling rates expected in Auckland and the largest particle diameter sizes ($< 110 \mu\text{m}$ mode) used in our research would cause disruption to road transportation from speed reduction due to visibility degradation ($< 600 \text{ m}$ visual ranges). Speed reduction in volcanic ashfall may be even greater than for fog due to additional transportation impacts such as road marking coverage by ash and reduced skid resistance (Wilson et al. 2012a; Wilson et al. 2014; Blake et al. 2016b, 2017a). In the absence of key research on driver behaviour in volcanic ashfall and

assuming no speed restrictions, based on data available for other atmospheric hazards we estimate an average free-flow speed of 30 km h^{-1} for a visual range of 5 m, with an increased chance of accidents due to lack of lane-keeping ability and obstructions hidden from view. With 20 m visual range, 50 km h^{-1} may be possible, but for the lowest expected visual ranges in Auckland ($\sim 1\text{--}2 \text{ m}$), driving is likely to become highly impractical and dangerous.

In an operational environment, transportation and emergency management officials may use knowledge of anticipated driver behaviour, along with results from our study and information on previous mitigation measures following historical eruptions (Table 1), to appropriately deal with reduced visibility (in addition to other impact types) from volcanic ash. For example, in dry conditions or during prolonged eruptions with recurring ashfalls, a 5-min spacing of road and rail vehicles may be appropriate as this allows $\sim 90\%$ of ash to settle (assuming no wind or other atmospheric disturbances). Additionally or alternatively, lower speed limits may be appropriate to minimise the resuspension of ash behind vehicles and reduce accident rates. Such mitigation measures align well with what was implemented on major routes following the 1980 Mount St Helens eruption; as Warrick (1981) states, “although the highways were officially closed, [vehicles] were allowed to proceed westward on I-90 and northward on US 97 at a rate of one vehicle every 5 min and a maximum speed of 25 mph” (p.21).

Transportation management policies and local regulations are likely to have a large influence on the level of disruption from volcanic ashfall in many locations. For example, in Auckland a “restricted visibility routine” for maritime area/s affected may come into effect when visibility of less than 1 nautical mile from a vessel’s bridge is encountered (AC 2014). This would have implications for the numbers and types of vessels permitted in certain areas, and their speeds (AC 2014; MNZ 2015). For airport operations at Auckland Airport, assuming no preceding closure due to other factors such as potential damage to aircraft engines, the visual ranges expected from most initial ashfalls mean that low visibility procedures would be initiated (triggered by $< 1500 \text{ m}$ visual range) (CAA 2008). Only essential ground support traffic directly involved with the arrival or departure of an aircraft will be allowed to operate in the manoeuvring area during such conditions. As the runway at Auckland Airport is equipped with a Category III B Instrument Landing System, aircraft and pilots with the appropriate ratings can land if the visual range is $> 50 \text{ m}$ (Auckland Airport 2008), with a maximum of six aircraft take-off and landing movements per hour (CAA 2008). With lower visual ranges, operations at the airport would cease, although closure would likely be necessary due to other factors by this stage.

6 Conclusions

We have developed an experimental approach to allow the calculation of visual range from given ash-settling rates for a range of different volcanic ash samples with different particle size and compositional characteristics. We have also tested this approach using a selection of volcanic ash samples that represent a range of characteristics that can be expected in Auckland, New Zealand, from multiple sources.

Our results demonstrate that visibility decreases with increasing ash-settling rate. Ash particle size has the greatest effect on visual range. For a given settling rate, fine-grained ash causes a shorter visual range than coarse-grained ash, a finding that aligns with existing research involving other particulate types. The influence of ash type, colour and shape on

visual range reduction is not as clear-cut as for particle size. We conclude that samples with a higher proportion of irregular-shaped particles cause a greater reduction in visual range than those with more spherical shapes. Light-coloured ash such as rhyolite appears to result in lower visual ranges than dark-coloured ash such as basalt; a trend that may be explained on the basis of increased reflection off light-coloured surfaces. However, further laboratory or field-based studies are required to confirm the true extent that particle colouration and shape impacts visual range.

We emphasise that our results are for initial volcanic ashfall only and that any remobilised and resuspended ash from fall deposits could cause lower visual ranges for extended periods of time post-eruption, exacerbating impacts to transportation. Our study highlights the need for rapid syn-eruptive and reliable measurements or calculations of airborne metrics including particle concentration, ash-settling rate and visual range. It also demonstrates the importance of considering different ash properties besides ash thickness in volcanic eruptions, including particle size distribution, shape and colour.

Contemporary ash dispersion and fallout models, which provide outputs of airborne ash concentration and/or ash-settling rate given particular eruptions, can be used to produce scenarios of transportation disruption from reduced visibility, as well as other assessments including for human and animal health hazards. In conjunction with scenarios for other impact types (e.g. reduced skid resistance and line marking coverage by ash), the findings enable the improvement of transportation management strategies during and following future volcanic ashfall.

Acknowledgements We acknowledge the support of the University of Canterbury Department of Geological Sciences, for (a) capex funding for the *TOPAS SAG-410 solid aerosol generator* (ash disperser) and *DynOptic DSL-460 MkII transmissometer* for experimentation; and (b) technical laboratory work support from Peter Jones, Rob Spiers, Chris Grimshaw, Matt Cockcroft, Sacha Baldwin-Cunningham, Cathy Higgins, Sarah Pope, Connor Jones and Stephen Brown, who we gratefully thank. Additionally, we thank the Chartered Institute of Logistics and Transport (CILT) for their financial contribution towards equipment costs. Funding support for the authors from the New Zealand Earthquake Commission (EQC), Determining Volcanic Risk in Auckland (DEVORA) project, Natural Hazards Research Platform (NHRP) and University of Canterbury Mason Trust is also greatly appreciated. We also acknowledge and appreciate the technical support provided by Stephan Große of TOPAS GmbH as well as Jozua Taljaard and Andrew Blair of Ecotech NZ Environmental for the operation and adaptations of the ash disperser and transmissometer, respectively. Daniel Blake would also like to thank his other PhD supervisors, Natalia Deligne (GNS Science), Jan Lindsay (The University of Auckland) and Jim Cole (University of Canterbury), for their edits, guidance and advice throughout the project. Additionally, we thank the two anonymous reviewers for critical review of this paper, which guided subsequent improvements.

Open Access This article is distributed under the terms of the Creative Commons Attribution 4.0 International License (<http://creativecommons.org/licenses/by/4.0/>), which permits unrestricted use, distribution, and reproduction in any medium, provided you give appropriate credit to the original author(s) and the source, provide a link to the Creative Commons license, and indicate if changes were made.

References

- Abdel-Aty M, Akram A, Huang H, Choi K (2011) A study on crashes related to visibility obstruction due to fog and smoke. *Accid Anal Prev* 43(5):1730–1737
- AC (2014) Harbourmaster's Office operation of vessels during periods of restricted visibility: navigation safety operating requirements. Auckland Council, Auckland
- AccuWeather (2015) First Calbuco eruption in 42 years suspends flights in Buenos Aires. AccuWeather.-com. <http://www.accuweather.com/en/weather-news/more-than-4000-evacuated-after/46042985>. Accessed 23 Nov 2015

- Adams C (2013) Identification of tuff rings in the Auckland Volcanic Field using LiDAR and ground penetrating radar. *New Zealand Journal of Geology and Geophysics*. <http://frontiersabroad.com/wp-content/uploads/2014/03/Cameron-Adams.pdf>. Accessed 08 June 2016
- Alloway B, Westgate J, Pillans B, Pearce N, Newnham R, Byrami M, Aarburg S (2004) Stratigraphy, age and correlation of middle Pleistocene silicic tephra in the Auckland region, New Zealand: a prolific distal record of Taupo Volcanic Zone volcanism. *NZ J Geol Geophys* 47:447–479
- Andò B, Baglio S, Marletta V (2014) Selective measurement of volcanic ash flow-rate. *IEEE Transact Instrum Measurement* 63(5):1356–1363
- Aplin K, Houghton I, Nicoll K, Humphries M, Tong A (2014) Electrical charging of volcanic ash. In: Proceedings of the ESA annual meeting on electrostatics. http://www.electrostatics.org/images/ESA_2014_G_Aplin_et_al.pdf. Accessed 10 Mar 2016
- Aplin K, Nicoll K, Houghton I (2015) Electrical charging of volcanic ash from Eyjafjallajökull. In: Geophysical research abstracts, 17, EGU General assembly 2015
- APTI (2000) OS 411: Computational atmospheric sciences. Air Pollution Training Institute, Shodor Education Foundation Inc., US EPA. <https://www.shodor.org/os411/index.html>. Accessed 27 Feb 2016
- Ashley WS, Strader S, Dziubla DC, Haberlie A (2015) Driving blind: weather-related vision hazards and fatal motor vehicle crashes. American Meteorology Society, Northern Illinois University. <http://journals.ametsoc.org/doi/pdf/10.1175/BAMS-D-14-00026.1>. Accessed 07 Apr 2016
- Auckland Airport (2008) Newsroom: fog at Auckland Airport and Category IIIB, 19 November 2008, Auckland Airport. http://www.aucklandairport.co.nz/~media/3FF843A AFCBB4C23B941EAA7406EAB7B.ashx?sc_database=web. Accessed 19 Mar 2016
- Barnard S (2009) The vulnerability of New Zealand lifelines infrastructure to ashfall. PhD Thesis, Hazard and Disaster Management, University of Canterbury, Christchurch, New Zealand
- Barsotti S, Neri A, Scire JS (2008) The VOL-CALPUFF model for atmospheric ash dispersal: 1. approach and physical formation. *J Geophys Res* 113:12p
- Barsotti S, Andronico D, Neri A, Del Carlo P, Baxter PJ, Aspinall WP, Hincks T (2010) Quantitative assessment of volcanic ash hazards for health and infrastructure at Mt. Etna (Italy) by numerical simulation. *J Volcanol Geoth Res* 192:85–96
- Bartney B (1980) Showers of muddy ash fall from fresh eruption. *The Lawrence Daily: Journal—World, Kansas*, 26 May 1980, vol 122, p 20
- Baxter P, Horwell CJ (1999) Impacts of eruptions on human health. In: Siggurdson H (ed) *Encyclopedia of Volcanoes*, 2nd edn. Academic Press, New York
- Binkowski FS, Roselle SJ, Mebest MR, Eder BK (2002) Modeling atmospheric particulate matter in an air quality modelling system using a modal method. In: Chock DP, Carmichael GR (eds) *Atmospheric modelling. The IMA Volumes in Mathematics and its Applications*, vol 130. Springer
- Blake DM, Wilson G, Stewart C, Craig HM, Hayes JL, Jenkins SF, Wilson TM, Horwell CJ, Andreastuti S, Daniswara R, Ferdiwijaya D, Leonard GS, Hendrasto M, Cronin S (2015) The 2014 eruption of Kelud volcano, Indonesia: impacts on infrastructure, utilities, agriculture and health. *GNS Sci Rep* 2015(15):139p
- Blake DM, Wilson TM, Deligne NI, Lindsay JL, Cole JW (2016a) Impacts of volcanic ash on road transportation: considerations for resilience in central Auckland. In: Proceedings paper for the Institute of Professional Engineers New Zealand (IPENZ) transportation group conference (March 2016), Auckland, New Zealand
- Blake DM, Wilson TW, Gomez C (2016b) Road marking coverage by volcanic ash: an experimental approach. *Environ Earth Sci* 75:1348
- Blake DM, Wilson TM, Cole JW, Deligne NI, Lindsay JM (2017a) Impact of volcanic ash on road and airfield surface skid resistance. *Sustainability* 9:1389
- Blake DM, Deligne NI, Wilson TM, Wilson G (2017b) Improving volcanic ash fragility functions through laboratory studies: example of surface transportation networks. *Journal of Applied Volcanology* 6:16
- Blong RJ (1982) The time of darkness: local legends and volcanic reality in Papua New Guinea. Australian National University Press, Canberra
- Blong RJ (1984) *Volcanic hazards: a sourcebook on the effects of eruptions*. Academic Press, Sydney
- Bonadonna C, Houghton B (2005) Total grain-size distribution and volume of tephra-fall deposits. *Bull Volc* 67:441–456
- Bonadonna C, Phillips J (2003) Sedimentation from strong volcanic plumes. *J Geophys Res Solid Earth* 108:B7
- Bonadonna C, Ernst GGJ, Sparks RSJ (1998) Thickness variations and volume estimates of tephra fall deposits: the importance of particle Reynolds number. *J Volcanol Geoth Res* 81:173–187
- Bonadonna C, Mayberry GC, Calder ES, Sparks RSJ, Choux C, Jackson P, Lejeune AM, Loughlin SC, Norton GE, Rose WI, Ryan G, Young SR (2002) Tephra fallout in the eruption of Soufrière Hills

- Volcano, Montserrat. In: Druitt TH, Kokelaar BP (eds) The eruption of Soufrière Hills Volcano, Montserrat, from 1995 to 1999, vol 21. Geological Society, London, pp 483–516
- Bonadonna C, Genco R, Gouhier M, Pistolesi M, Cioni R, Alfano F, Hoskuldsson A, Ripepe M (2011) Tephra sedimentation during the 2010 Eyjafjallajökull eruption (Iceland) from deposit, radar, and satellite observations. *J Geophys Res* 116:B12202
- Bonasia R, Costa A, Folch A, Capra L, Macedonio G (2012) Numerical simulation of tephra transport and deposition of the 1982 El Chichon eruption and implications for hazard assessment. *J Volcanol Geoth Res* 231–232:39–49
- Brazier S, Davis AN, Sigurdsson H, Sparks RSJ (1982) Fall-out and deposition of volcanic ash during the 1979 explosive eruption of the Soufriere of St. Vincent. *J Volcanol Geoth Res* 14:335–359
- Brooks JO, Crisler MC, Klein N, Goodenough R, Beeco RW, Guirl C, Tyler PJ, Hilpert A, Miller Y, Grygier J, Burroughs B, Martin A, Ray R, Palmer C, Beck C (2011) Speed choice and driving performance in simulated foggy conditions. *Accid Anal Prev* 43(3):698–705
- Broom SJ (2010) Characterisation of “pseudo-ash” for quantitative testing of critical infrastructure components with a focus on roofing fragility. BSc (Hons) Thesis, Hazard and Disaster Management, University of Canterbury, Christchurch, New Zealand
- CAA (2008) Low visibility operations at Auckland Airport. Vector: pointing to safer aviation, Issue 4, Civil Aviation Authority of New Zealand. https://www.caa.govt.nz/Publications/.../Vector_2007_Issue4_JulAug.pdf. Accessed 19 Mar 2016
- Carey S, Bursik M (2015) Volcanic plumes. In: Sigurdsson H (ed) Encyclopedia of Volcanoes. Academic Press, New York, pp 571–585
- Carey S, Sigurdsson H (1982) Influence of particle aggregation on deposition of distal tephra from the May 18, 1980 eruption of Mount St. Helens Volcano. *J Geophys Res* 87(B8):7061–7072
- Carey S, Sigurdsson H (1986) The 1982 eruptions of El Chichon volcano, Mexico (2): observations and numerical modelling of tephra-fall distribution. *Bull Volc* 48:127–141
- Cassidy J, Locke C (2004) Temporally linked volcanic centres in the Auckland Volcanic Field. *NZ J Geol Geophys* 47:287–290
- Codling JP (1971) Thick fog and its effect on traffic flow and accidents. In: Transport and road research laboratory TRRL report LR 397, TRRL, Crowthorne
- Cole J, Blumenthal E (2004) Evacuate!: what an evacuation order given because of a pending volcanic eruption could mean to residents of the Bay of Plenty. Tephra, June 2004. Natural Hazards Research Centre, University of Canterbury, Christchurch
- Conner WD (1974) Measurement of opacity and mass concentration of particulate emissions by transmissometry, EPA 650/2-74-128. United States Environmental Protection Agency, Washington, D.C
- Conner WD, Knapp KT, Nader JS (1979) Applicability of transmissometers to opacity measurement of emissions—oil-fired power plants and Portland cement plants, EPA 600/2-79-188. United States Environmental Protection Agency, Washington, D.C
- Costa A, Macedonio G, Folch A (2006) A three-dimensional Eulerian model for transport and deposition of volcanic ashes. *Earth Planet Sci Lett* 241(3–4):634–647
- Costa A, Dell’Erba F, Di Vito MA, Isaia R, Macedonio G, Orsi G, Pfeiffer T (2009) Tephra fallout hazard assessment at the Campi Flegrei caldera (Italy). *Bull Volc* 71(3):259–273
- Cova TJ, Conger S (2003) Transportation hazards. In: Kutz M (ed) Handbook of transportation engineering. McGraw-Hill Handbook, New York City
- Craig H, Wilson T, Stewart C, Outes V, Villarosa G, Baxter P (2016) Impacts to agriculture and critical infrastructure in Argentina after ashfall from the 2011 eruption of the Cordón Caulle volcanic complex: an assessment of published damage and function thresholds. *J Appl Volcanol* 5(7):31p
- Durant AJ, Rose WI, Sarna-Wojcicki AM, Carey S, Volentik AC (2009) Hydrometeor-enhanced tephra sedimentation from the 18 May 1980 Mount St. Helens (USA) volcanic cloud. *J Geophys Res* 114:B03204
- DynOptic (ed) (2014) DSL-460 double pass opacity/dust monitor: operators manual v1.4. DynOptic Systems Ltd, Brackley
- Edwards JB (1999) Speed adjustment of motorway commuter traffic to inclement weather. *Transp Res Part F* 2:1–14
- Electrostatic Solutions Ltd. (2000) Electrostatic solutions technical brief No. 6: triboelectrification—how materials charge by contact. Hampshire, UK. <http://www.electrostatics.net/pdf/TB6-triboelectrification.pdf>. Accessed 15 May 2016
- Elliot AJ, Singh N, Loveridge P, Harcourt S, Smith S, Pnaiser R, Kavanagh K, Robertson C, Ramsay CN, McMenamin J, Kibble A, Murray V, Ibbotson S, Catchpole M, McCloskey B, Smith GE (2010) Syndromic surveillance to assess the potential public health impact of the Icelandic volcanic ash plume across the United Kingdom, April 2010. *Eurosurveillance* 15(23)

- EPA (2000) Current knowledge of particulate matter (PM) continuous emission monitoring: final report. United States Environmental Protection Agency. <https://www3.epa.gov/ttnemc01/cem/pmcemsknowfinalrep.pdf>. Accessed 14 Mar 2016
- EPA (2001) Protecting visibility: an EPA report to congress, chapter 3. United States Environmental Protection Agency. <http://www.epa.gov/nscep>. Accessed 06 Mar 2016
- Eto T (2001) Estimation of amount and dispersal volcanic ash-fall deposits ejected by vulcanian type eruption. *Rep Fac Sci Kagoshima Univ* 34:35–46
- Fagents SA, Gregg TKP, Lopes RMC (2013) Modelling volcanic processes: the physics and mathematics of volcanism. Cambridge University Press, Cambridge
- Folch A (2012) A review of tephra transport and dispersal models: evolution, current status, and future perspectives. *J Volcanol Geoth Res* 235–236:96–115
- Folch A, Sulpizio R (2010) Evaluating long-range volcanic ash hazard using supercomputing facilities: application to Somma-Vesuvius (Italy), and consequences for civil aviation over the Central Mediterranean area. *Bull Volc* 72:1039–1059
- Folch A, Costa A, Macedonia G (2009) FALL3D: a computational model for transport and deposition of volcanic ash. *Comput Geosci* 35:1334–1342
- Folch A, Costa A, Durant A, Macedonio G (2010) A model for wet aggregation of ash particles in volcanic plumes and clouds: 2. Model application. *J Geophys Res Chem Phys Miner Rocks Volcanol* 115:B9
- Folch A, Mingari L, Osoreo MS, Collini E (2014) Modeling volcanic ash resuspension—application to the 14–18 October 2011 outbreak episode in central Patagonia, Argentina. *Nat Hazards Earth Syst Sci* 14:119–133
- Fowler WB, Lopushinsky W (1986) Wind-blown volcanic ash in forest and agricultural locations as related to meteorological conditions. *Atmos Environ* 20(3):421–425
- Jenkins S, Wilson T, Magill C, Miller V, Stewart C, Warner M, Boulton M (2014) Volcanic ash fall hazard and risk. UN-ISDR 2015 Global Assessment Report on Disaster Risk Reduction Technical Background Paper, United Nations Office for Disaster Risk Reduction. <https://www.unisdr.org/we/inform/publications/49769>. Accessed 09 Feb 2018
- Guffanti M, Mayberry GC, Casadevall TJ, Wanderman R (2009) Volcanic hazards to airports. *Nat Hazards* 51:287–302
- GVP (2013) Report on San Cristobal (Nicaragua): January 2013. Global Volcanism Program. <http://volcano.si.edu/showreport.cfm?doi=10.5479/si.GVP.BGVN201301-344020>. Accessed 23 Nov 2015
- Hagen LJ, Skidmore EL (1977) Wind erosion and visibility problems. *Trans Am Soc Agric Eng* 20(5):898–903
- Hardy SEJ (2015) Major incident in Kent: a case report. *Scand J Trauma Resusc Emerg Med* 23(71)
- Harris DM, Rose WI (1983) Estimating particle sizes, concentrations, and total mass of ash in volcanic clouds using weather radar. *J Geophys Res* 88(C15):10969–10983
- Hill DJ (2014) Filtering out the ash: mitigating volcanic ash ingestion for generator sets. Masters Thesis, Hazard and Disaster Management, University of Canterbury, Christchurch, New Zealand
- Hincks TK, Aspinall WP, Baxter PJ, Searl A, Sparks RSJ, Woo G (2006) Long term exposure to respirable volcanic ash on Montserrat: a time series simulation. *Bull Volc* 68:266–284
- Hitchcock DW, Cole JW (2007) Potential impacts of a widespread subplinian andesitic eruption from Tongariro volcano, based on a study of the Poutu Lapilli. Department of Geological Sciences, University of Canterbury, Christchurch
- Horwell CJ (2007) Grain-size analysis of volcanic ash for the rapid assessment of respiratory health hazards. *J Environ Monit* 9:1107–1115
- Howe T, Lindsay JM, Mortimer N, Leonard G (2011) DEVORA borehole database: status update and manual, IESE Report 1-2011.03. Institute of Earth Science and Engineering, Auckland, New Zealand
- Hyslop N (2009) Impaired visibility: the air pollution people see. *Atmos Environ* 43(1):182–195
- Ibrahim D (2015) Massive dust storm triggers deadly pileup in Colorado. The Weather Network. <http://www.theweathernetwork.com/us/news/articles/massive-dust-storm-triggers-deadly-pileup-in-colorado/52592/>. Accessed 18 Jan 2016
- Johnston DM (1997) Physical and social impacts of past and future volcanic eruptions in New Zealand. PhD Thesis, Earth Science, Massey University, Palmerston North, New Zealand
- Kienle J, Swanson SE (1985) Volcanic hazards from future eruptions of Augustine Volcano. University of Alaska Geophysical Institute, Alaska
- Komer PD, Reimers CE (1978) Grain shape effects on settling rates. *J Geol* 86:193–209
- Koschmieder H (1925) Theorie der horizontalen Sichtweite, Keim and Nennich
- Lara LE (2009) The 2008 eruption of the Chaitén Volcano, Chile: a preliminary report. *Andean Geol* 36(1):125–129

- Leonard GS, Stewart C, Wilson TM, Proctor JN, Scott BJ, Keys HJ, Jolly GE, Wardman JB, Cronin SJ, McBride SK (2014) Integrating multidisciplinary science, modelling and impact data into evolving, syn-event volcanic hazard mapping and communication: a case study from the 2012 Tongariro eruption crisis, New Zealand. *J Volcanol Geoth Res* 286:208–232
- Leonard GS, Calvert AT, Hopkins J, Wilson CJL, Smid ER, Lindsay JM, Champion DE (2017) High-precision $^{40}\text{Ar}/^{39}\text{Ar}$ dating of Quaternary basalts from Auckland Volcanic Field, New Zealand, with implications for eruption rates and paleomagnetic correlations. *J Volcanol Geoth Res* 343:60–74
- Lindsay JM, Peace C (2005) Project AELG-7: health and safety issues in a volcanic ash environment. In: Auckland Regional Council Technical Publication 290, Auckland Engineering Lifelines Group
- Macedonio G, Costa A, Scollo S, Neri A (2016) Effects of eruption source parameter variation and meteorological dataset on tephra fallout hazard assessment: example from Vesuvius (Italy). *J Appl Volcanol* 5:5
- Magill C, Wilson T, Okada T (2013) Observations of tephra fall impacts from the 2011 Shinmoedake eruption, Japan. *Earth Planet Space* 65:677–698
- Malm W (1979) Visibility: a physical perspective. In: Fox D, Loomis RJ, Greene TC (eds). In: Proceedings of the workshop in visibility values. U.S. Department of Agriculture, Fort Collins, Colorado 56–68
- Malm CW, Day DE, Kreidenweis SM, Collett JL, Lee T (2003) Humidity-dependent optical properties of fine particles during the Big Bend Regional Aerosol and Visibility Observational Study. *J Geophys Res* 108:D9
- MFE (2001) Good practice guide for monitoring and management of visibility in New Zealand. Ministry for the Environment Report, Wellington
- Miwa T, Nagai M, Kawaguchi R (2018) Resuspension of ash after the 2014 phreatic eruption at Ontake volcano Japan. *J Volcanol Geoth Res* 351:105–114
- MNZ (2015) Maritime Rules Part 22: collision prevention. Maritime New Zealand, Wellington, New Zealand. <https://www.maritimenz.govt.nz/Rules/Rule-documents/Part22-maritime-rule.pdf>. Accessed 19 Mar 2016
- Moen WS (1981) Physical and chemical properties of ash from the May 18, 1980, eruption of Mount St. Helens. In: Moen WS, McLucas GB (eds) Mount St. Helens Ash—properties and possible Uses, report of investigations 24, Washington Department of Natural Resources, Division of Geology and Earth Resources
- Moore RL, Cooper L (1972) Fog and road traffic. Transport and Road Research Laboratory. In: TRRL Report LR 446, TRRL, Crowthorne
- Mueller AS, Trick LM (2012) Driving in fog: the effects of driving experience and visibility on speed compensation and hazard avoidance. *Accid Anal Prev* 48:472–479
- Musk L (1991) Climate as a factor in the planning and design of new roads and motorways. In: Perry AH, Symons LJ (eds) Highway Meteorology. E. & F.N. Spon, London
- OECD (1986) Road Safety Research 1986. OECD, Paris
- Pardini F, Spanu A, Vitturi MM, Salvetti MV, Neri A (2016) Grain size distribution uncertainty quantification in volcanic ash dispersal and deposition from weak plumes. *J Geophys Res Solid Earth* 121(2):538–557
- Parfitt L, Wilson L (2009) Fundamentals of Physical Volcanology. In: Sigurdsson H (ed) Encyclopedia of Volcanoes. Academic Press, Cambridge
- Perry AH (1981) Environmental hazards in the British Isles. George Allen and Unwin, London
- Pyle DM (1989) The thickness, volume and grainsize of tephra fall deposits. *Bull Volc* 51:1–15
- Reckziegel F, Bustos E, Mingari L, Báez W, Villarosa G, Folch A, Collini E, Viramonte J, Romero J, Osoreo S (2016) Forecasting volcanic ash dispersal and coeval resuspension during the April–May 2015 Calbuco eruption. *J Volcanol Geoth Res* 321:44–57
- Riley CM, Rose WI, Bluth GJS (2003) Quantitative shape measurements of distal volcanic ash. *J Geophys Res* 108:B10
- Robinson E (1968) Effect on the physical properties of the atmosphere. In: Stern AC (ed) Air Pollution, 1:2. Academic Press, New York, pp 349–400
- Rose WI, Durant AJ (2009) Fine ash content of explosive eruptions. *J Volcanol Geoth Res* 186:32–39
- Sahetapy-Engel S, Self S, Carey RJ, Nairn IA (2014) Deposition and generation of multiple widespread fall units from the c. AD 1314 Kaharoa rhyolitic eruption, Tarawera, New Zealand. *Bull Volc* 76:836
- Sarkinen CF, Wiitala JT (1981) Investigation of volcanic ash on transmission facilities in the Pacific Northwest. *IEEE Trans Power Appar Syst* 5:2278–2286
- Sarna-Wojcicki AM, Shipley S, Waitt RB, Dzurisin D, Wood SH (1981) Areal distribution, thickness, mass, volume, and grain size of air-fall ash from six major eruptions of 1980. In: Lipman PW, Mullineaux DR (eds) The 1980 eruptions of Mount St. Helens, Washington, USGS Professional Paper 1250, pp 577–600

- Scasso RA, Corbella H, Tiberi P (1994) Sedimentological analysis of the tephra from the 12–15 August 1991 eruption of Hudson volcano. *Bull Volcanol* 56:121–132
- Scheidegger KF, Federman AN (1982) Compositional heterogeneity of tephra from the 1980 eruptions of Mount St. Helens. *J Geophys Res* 87(B13):10861–10881
- Scollo S, Del Carlo P, Coltelli M (2007) Tephra fallout of 2001 Etna flank eruption: analysis of the deposit and plume dispersion. *J Volcanol Geoth Res* 160:147–164
- Scollo S, Folch A, Costa A (2008) A parametric and comparative study of different tephra fallout models. *J Volcanol Geoth Res* 176(2):199–211
- Scott WE, McGimsey RG (1994) Character, mass, distribution, and origin of tephra-fall deposits of the 1989–1990 eruption of Redoubt Volcano, south-central Alaska. *J Volcanol Geoth Res* 62:251–272
- Searl A, Nicholl A, Baxter PJ (2002) Assessment of the exposure of islanders to ash from the Soufriere Hills volcano, Montserrat, British West Indies. *Occup Environ Med* 59:523–531
- Seinfeld JH, Pandis SN (2006) Atmospheric chemistry and physics: from air pollution to climate change. Wiley, Hoboken
- Self S, Sparks RSJ, Booth B, Walker GPL (1974) The 1973 Heimaey Strombolian scoria deposit, Iceland. *Geol Mag* 111(6):539–548
- Shimano T, Nishimura T, Nobuyuki C, Shibasaki Y, Iguchi M, Miki D, Yokoo A (2013) Development of an automatic volcanic ash sampling apparatus for active volcanoes. *Bull Volcanol* 75:773
- Sigurdsson H, Carey S, Cornell W, Pescatore T (1985) The eruption of Vesuvius in AD 79. *Natl Geogr Res* 1:332–387
- Sivakumar MVK (2005) Impacts of sand storms/dust storms on agriculture. In: Sivakumar MVK, Motha RP, Das HP (eds) Natural disasters and extreme events in agriculture. Springer, Berlin, pp 159–177
- Smith IEM, Allen SR (1993) Volcanic hazards: Auckland Volcanic Field. Department of Geology, University of Auckland, Auckland
- Sparks R (1986) The dimensions and dynamics of volcanic eruption columns. *Bull Volc* 48:3–15
- Sparks RSJ, Bursik MI, Ablay GJ, Thomas RME, Carey SN (1992) Sedimentation of tephra by volcanic plumes. Part 2: controls on thickness and grain-size variations of tephra fall deposits. *Bull Volc* 54:685–695
- Sparks RSJ, Bursik MI, Carey SN, Gilbert JS, Glaze LS, Sigurdsson H, Woods AW (1997) Volcanic plumes. Wiley, Hoboken
- Statistics New Zealand (2015) Subnational population estimates. <http://nzdotstat.stats.govt.nz/wbos/Index.aspx?DataSetCode=TABLECODE7502>. Accessed 31 Aug 2016
- Stohl A, Hittenberger M, Wotawa G (1998) Validation of the Lagrangian particle dispersion model FLEXPART against large scale tracer experiments. *Atmos Environ* 32:4245–4264
- Stohl A, Forster C, Frank A, Siebert P, Wotawa G (2005) Technical note: the Lagrangian particle dispersion model FLEXPART version 6.2. *Atmos Chem Phys* 5:2461–2474
- Summer R, Baguley C, Burton J (1977) Driving in fog on the M4. In: Transport and road research laboratory TRRL report LR 281, TRRL, Crowthorne
- Tajima Y, Ohara D, Fukuda K, Shimomura S (2015) Development of automatic tephrometer for monitoring of volcano. https://www.n-koei.co.jp/business/technology/library/thesis/pdf/forum23_005.pdf. Accessed 17 June 2016
- Tang IN (1996) Chemical and size effects of hygroscopic aerosols on light scattering coefficients. *J Geophys Res* 101:19245–19250
- Taylor JR, Moogan JC (2010) Determination of visual range during fog and mist using digital camera images. In: IOP conference series: earth and environmental science, 11. 17th national conference of the Australian meteorological and oceanographic society
- Thorarinsson S (1971) Damage caused by tephra fall in some big Icelandic eruptions and its relation to the thickness of tephra layers. In: Acta of the first international science congress on the Volcano of Thera, Greece, vol 1969, pp 15–23
- USDOT (2013) How do weather events impact roads? Weather Management Program. www.ops.fhwa.dot.gov/weather/q1_roadimpact.htm. Accessed 07 Apr 2016
- USGS (2013) Volcanic ash: effects and mitigation strategies. United States Geological Survey. <http://volcanoes.usgs.gov/ash/trans/>. Accessed 21 Sep 2015
- Uthe EE (1980) Evaluation of an infrared transmissometer for monitoring particulate mass concentrations of emissions from stationary sources. *J Air Pollut Control As* 30:382–386
- van de Hulst HC (1957) Light scattering by small particles. Wiley, New York
- Walker GPL (1981) The Waimihia and Hatepe plinian deposits from the rhyolitic Taupo Volcanic Centre. *NZ J Geol Geophys* 24(3):305–324
- Wardman J, Sword-Daniels V, Stewart C, Wilson T (2012) Impact assessment of the May 2010 eruption of Pacaya volcano, Guatemala. GNS Science Report 2012/09

- Warrick RA (1981) Four communities under ash. University of Colorado, Boulder, U.S, Institute of Behavioural Science
- Watt SFL, Pyle DM, Mather TA, Martin RS, Matthews NE (2009) Fallout and distribution of volcanic ash over Argentina following the May 2008 explosive eruption of Chaitén, Chile. *J Geophys Res* 114:B04207
- Weber K, Fischer C, Vogel A, Pohl T, Böhlke C (2013) First results of an airborne release of volcanic ash for testing of volcanic ash plume measurement instruments. In: *Proceedings of Energy and Environment*, pp 169–172
- Weinzierl B, Sauer D, Minikin A, Reitebuch O, Dahlkötter F, Mayer B, Emde C, Tegen I, Gasteiger J, Petzold A, Veira A, Kueppers U, Schumann U (2012) On the visibility of airborne volcanic ash and mineral dust from the pilot's perspective in flight. *Phys Chem Earth* 45–46:87–102
- White WH (1990) The components of atmospheric light extinction: a survey of ground-level budgets. *Atmos Environ* 24A:2673–2679
- White J, Stewart C, Wareham D, Wilson T (2011) Treatment of volcanic ash-contaminated surface waters through the optimisation of physical and chemical processes. *GNS Science Report* 2011/35
- WHO (2013) Review of evidence on health aspects of air pollution—REVIHAAP project: final technical report. World Health Organisation European Centre for Environment and Health, Bonn
- Wilcox RE (1959) Some effects of recent Volcanic Ash falls with especial reference to Alaska. *Geol Sur Bull* 1028-N. <https://pubs.usgs.gov/bul/1028n/report.pdf>. Accessed 09 Feb 2018
- Wilson TM (2008) Unpublished field notes from the Chaitén eruption field visit. University of Canterbury, Christchurch
- Wilson TM (2009) Unpublished field notes from the Hudson eruption field visit. University of Canterbury, Christchurch
- Wilson L, Huang TC (1979) The influence of shape on the atmospheric settling velocity of volcanic ash particles. *Earth Planet Sci Lett* 44:311–324
- Wilson TM, Stewart C, Cole JW, Dewar DJ, Johnston DM, Cronin SJ (2009) The 1991 eruption of Volcan Hudson, Chile: impacts on agriculture and rural communities and long-term recovery. *GNS Science Report* 2009/66
- Wilson TM, Cole JW, Stewart C, Cronin SJ, Johnston DM (2011) Ash storms: impacts of wind-remobilised volcanic ash on rural communities and agriculture following the 1991 Hudson eruption, southern Patagonia, Chile. *Bull Volc* 73:223–239
- Wilson TM, Stewart C, Sword-Daniels V, Leonard GS, Johnston DM, Cole JW, Wardman J, Wilson G, Barnard ST (2012a) Volcanic ash impacts on critical infrastructure. *Phys Chem Earth* 45–46:5–23
- Wilson T, Cole J, Johnston D, Cronin S, Stewart C, Dantas A (2012b) Short- and long-term evacuation of people and livestock during a volcanic crisis: lessons from the 1991 eruption of Volcan Hudson, Chile. *J Appl Volcanol* 1:2
- Wilson T, Stewart C, Bickerton H, Baxter P, Outes V, Villarosa G, Rovere E (2013) Impacts of the June 2011 Puyehue-Cordon Caulle volcanic complex eruption on urban infrastructure, agriculture and public health. *GNS Science Report* 2012/20
- Wilson G, Wilson TM, Deligne NI, Cole JW (2014) Volcanic hazard to critical infrastructure: a review. *J Volcanol Geoth Res* 286:148–182
- Wilson G, Wilson TM, Deligne NI, Blake DM, Cole JW (2017) Framework for developing volcanic fragility functions for critical infrastructure. *J Appl Volcanol* 6:14
- Witham C, Hort M, Potts R, Servranckx R, Husson P, Bonnardot F (2007) Comparison of VAAC atmospheric dispersion models using the 1 November 2004 Grimsvotn eruption. *Meteorol Appl* 14:27–38
- Yanagi T, Okada H, Ohta K (1992) Unzen volcano, the 1990–1992 eruption. The Nishinippon and Kyushu University Press, Fukuoka
- Zawalna-Geer A (2016) Towards a tephra framework for the Auckland maar lake sediments and the potential of applying cryptotephra techniques. PhD Thesis, Geology, The University of Auckland, Auckland, New Zealand